Spring 2017

In-situ assessment of concrete bridge decks and pavements using stress-wave based methods

Mengxing Li

IN-SITU ASSESSMENT OF CONCRETE BRIDGE DECKS AND PAVEMENTS USING STRESS-WAVE BASED METHODS

by

MENGXING LI

A DISSERTATION

Presented to the Faculty of the Graduate School of the

MISSOURI UNIVERSITY OF SCIENCE AND TECHNOLOGY

In Partial Fulfillment of the Requirements for the Degree

DOCTOR OF PHILOSOPHY

in

GEOLOGICAL ENGINEERING

2017

Approved

Neil L. Anderson, Advisor
Lesley H. Sneed
Norbert H. Maerz
David J. Rogers
Evgeniy V. Torgashov

PUBLICATION DISSERTATION OPTION

This dissertation has been prepared in journal publication format.

Paper I, pages 16-43, is entitled “Application of ultrasonic surface wave techniques for concrete bridge deck condition assessment,” and is prepared in the style used by the *Journal of Applied Geophysics* as published in volume 126, pp 148 -157 (March, 2016).

Paper II, pages 44-73, is entitled “Condition assessment of concrete pavements using both ground penetrating radar and stress-wave based techniques,” and is prepared in the style used by the *Journal of Applied Geophysics*, as published in volume 135, pp 297 - 308 (August, 2016).

Paper III, pages 74- 104, is entitled “An assessment of concrete over asphalt pavement using both the ultrasonic surface wave and impact echo techniques,” and is prepared in the style used by the *Journal of Environmental and Engineering Geophysics (JEEG)* as published in volume 21, No. 4, pp 137 – 149 (December, 2016).

ABSTRACT

Concrete infrastructure of United States is aging and deteriorating. Accurate assessment the condition of concrete infrastructure is critical for its maintenance and rehabilitation. Stress-wave based methods, including ultrasonic surface wave (USW) and impact echo (IE), are becoming popular for characterizing defects and mechanical properties of concrete infrastructures. In this dissertation, a comprehensive literature review of seismic wave theory and common types of defects identified in concrete infrastructures, as well as stress-wave based methods used for concrete infrastructure monitoring and characterizing on a selected concrete bridge deck and two concrete pavement segments are present. The utility and reliability of both methods were carefully evaluated and validated based on the comparison analysis with other destructive or non-destructive testing (NDT) methods carried out in the field or laboratory for the same bridge decks and pavement segments, such as the concrete hydro-demolition, drilling, static modulus of elasticity of concrete specimens in compression and ground penetrating radar (GPR). Detailed investigation of the sensitivity and limitation of stress-wave based methods for different types of defects identified in concrete bridge decks and pavements has been performed and presented. The outcome of this study is to expand the knowledge of stress-wave based methods, to better understand their strengths and limitations, to evaluate the reliability and utility of both the USW and IE test results in characterizing and monitoring defects and mechanical properties of concrete infrastructures. The result of this study is most beneficial for transportation agencies and researchers to use stress-wave based methods properly and effectively for further feasibility studies or monitoring of concrete infrastructures.

ACKNOWLEDGEMENTS

Undertaking this PhD has been a truly life-changing experience for me and it would not have been possible to do without the support and guidance that I received from many people.

First and foremost, I wish to thank my advisor, professor Neil L. Anderson, for all the support and encouragement he gave me during the time I spent at Missouri S&T. Without his guidance and constant feedback this PhD would not have been achievable. Many thanks also to my dissertation committee members, thank you to Lesley H. Sneed, David J. Rogers, Norbert H. Maerz and Torgashov V. Evgeniy for being my major advisors.

I gratefully acknowledge the funding received towards my PhD research work from the Missouri Department of Transportation (#TRyy1308 and #TRyy1141) and the U.S. Department of Transportation (#DTRT06-G-0014). I am also grateful to the funding received through the National University Transportation Center (NUTC) at Missouri S&T (#00039112).

My deep appreciation goes out to the applied geophysics lab members at Missouri S&T: Stanley, Adel, Aleksey and Sasha. Their excellent work and support during field data collection has made an important contribution towards my PhD.

Finally, I would like to thank my family for all their love and support. For my parents, Hongxia and Dexin, who raised me with a love of science and support me to chase my dreams. And most of all for my loving, supportive and patient wife Ming Yi, who has been by my side throughout this PhD. Without her support and courage this PhD work would not have been completed.

TABLE OF CONTENTS

Page

LIST OF ILLUSTRATIONS

PAPER II

LIST OF TABLES

1. INTRODUCTION

Concrete infrastructure of United States is aging and deteriorating. Accurate assessment the condition of concrete infrastructure is critical for its maintenance and rehabilitation. In the past two decades, non-destructive testing (NDT) methods have been widely used for this purpose since they are in-situ, rapid, non-destructive and accurate compared with the traditional drilling or laboratory testing methods. Based on overall value, accuracy, ease of use and cost, the stress-wave based methods, such as the ultrasonic surface wave (USW) and impact echo (IE), are two widely used and promising techniques (Gucunski *et al.,* 2013; Sneed *et al.,* 2014; Anderson *et al.,* 2015). Both USW and IE methods are based on generation of stress-waves and measurement of their propagation velocities and other characteristics, such as reflection and dispersion. The USW method is used to measure the in-situ elastic modulus (dynamic modulus) of the material and the IE method is used to locate defects as well as measure the thickness of the tested object (Baker *et al.,* 1997; Cheng and Sansalone, 1993).

The spectral analysis of surface wave (SASW) method was first introduced in early 1980's as a nondestructive test (NDT) method to determine in-suit elastic modulus of pavements (Nazarian, 1984; Nazarian and Stoke, 1986). In order to improve the data acquisition speed and overcome some inherit limitations of SASW method, the ultrasonic surface wave (USW) method was introduced in early 1990's (Baker *et al.,* 1995). In USW method, the frequency range of interest is limited to a high-frequency range where the surface wave's penetration depth is less than the thickness of the tested object. With the development of test instrument and computational software, the USW method has been successfully used to measure in-situ elastic modulus and monitor new or old

concrete structures in many cases (Baker *et al.,* 1997; Nazarian *et al.,* 1997; Celaya *et al.*, 2007; Li *et al.,* 2016). On the other hand, the impact-echo (IE) method was first introduced in early 1980's as anther nondestructive testing (NDT) method to determine internal flaws of concrete structures and measure their thickness (Carino *et al.*, 1986a). Since then, the IE method has been successfully used to monitor different type of concrete structures in many cases (Carino and Sansalone, 1990; Lin and Sansalone, 1996; Sansalone and Streett, 1997). In 1997, the IE method has been approved as the standard test method for measuring the P-wave speed and the thickness of concrete plates by American Society of Testing Materials (ASTM C1383). With the development of test instruments and computational software, non-contact air coupled sensor was introduced and improved the acquisition speed of IE method on plate-likely concrete structures (Zhu and Popovics, 2007; Zhu and Popovics, 2008).

Although the stress-wave based NDT methods has been widely used for monitoring concrete structures in many cases, most state transportation agencies still do not use it on a regular basis for monitoring and characterizing the condition of concrete infrastructures, such as bridge decks or pavements. Part of the reason is the complexity of data interpretation, especially when the existence of a potential defect is involved. Recent experimental studies conducted on both IE and USW methods indicates that the effectiveness of these NDT methods is limited by their sensitivity to different parameters, such as the defects size and depth, boundary conditions or material properties (Azari, 2013; Azari and Nazarian, 2015).

In order to help the state transportation agencies and civil engineers gain a better understanding of the relations and interactions between the data results of stress-wave

based methods and the deterioration conditions of concrete structures, in this study, a combination of stress-wave based methods (USW and IE) were used to monitor and characterize the condition of selected eleven bridge decks and eight pavements segments with different deterioration conditions in multiple locations of the state of Missouri. Other NDT and destructive testing methods, such as the Light detection and ranging (LiDAR), ground penetrating radar (GPR) and the traditional drilling methods were also conducted at each test site in order to compare and confirm with both USW and IE test results.

The contribution of this study is to expand the knowledge of stress-wave based methods, to better understand their potentials and limitations, to evaluate the reliability and accuracy of both the USW and IE methods in deterioration detection and material characterization of concrete infrastructures. The result of this research study will be most beneficial for transportation agencies and researchers to use both the USW and IE methods properly and effectively in further feasibility studies or investigations of concrete infrastructures.

Section 1 provide a literature review of both the USW and IE methods for concrete infrastructures evaluation. Then, the basic principles of stress-waved methods and seismic wave propagation theory are introduced. Finally, the fundamental principles of both the USW and IE methods are briefly introduced. Common defects characterized in concrete bridge decks and pavements are also briefly introduced.

Paper I present the results obtained from a study to evaluate the potentials and limitations of the USW method for detecting the concrete degradation and deck delamination induced by corrosion of embedded reinforcing steel on a concrete bridge

deck. The information of the size and depth of concrete deck delamination and degradation was exposed by hydro-demolition process and used to evaluate the performance of the USW method.

Paper II presents the results obtained from a study to evaluate the potentials and limitations of both the USW and IE methods for detecting the fine air voids under a single layered concrete pavement segment. The performance of both stress-waved based methods was then confirmed and compared with ground penetrating radar and traditional drilling results obtained at nearby locations.

Paper III investigates the accuracy and reliability of both the USW and IE methods for detecting the debonding and stripping embedded in a multiple layered pavement segment. The performance of both stress-waved based methods was then confirmed and compared with traditional drilling and laboratory test results obtained at nearby locations.

Section 2 presents a summary and conclusion obtained from above three individual research studies. It also provides recommendations for further studies.

1.1 BASIC PRINCIPLES OF STRESS-WAVE BASED METHODS

1.1.1 Wave Types. When a disturbance (stress or displacement) is applied on the surface of a test object, three types of stress-waves are generated: compressional wave (P-wave), shear wave (S-wave) and surface wave (R-wave) (Carino, 2001). The P-wave and S-wave propagate into the test object along spherical wave fronts (Figure 1.1). The P-wave is associated with the propagation of compressional stress (parallel to the direction of wave fronts) and S-wave is associated with shear stress (perpendicular to the direction

of wave fronts). On the other hand, the R-wave travels away from the disturbance along the surface of test object.

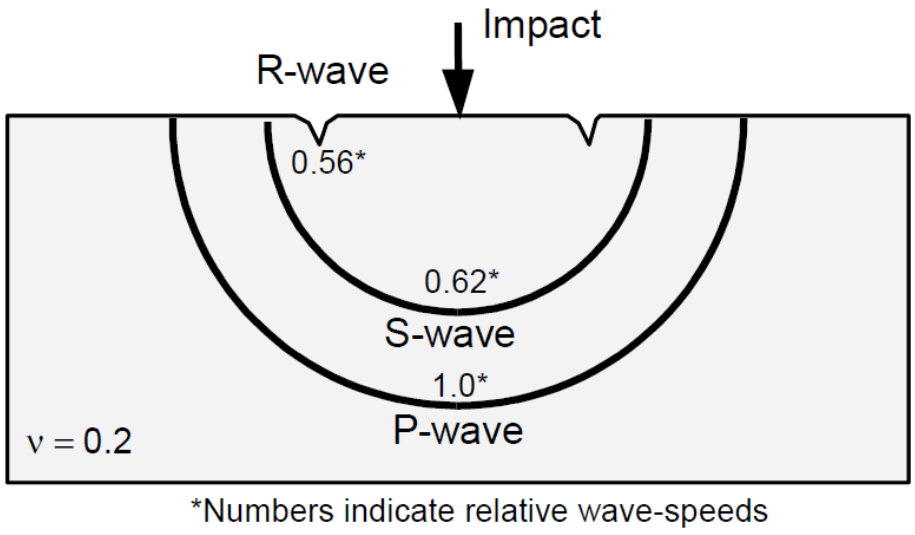

Figure 1.1 Stress-Waves caused by Impact at a Point on the Surface of an Object (adapted from Carino, 2001)

1.1.2 Wave Speed. In infinite elastic solids, the P-wave speed (V_p) is a function of Young's modulus of elasticity, *E*, the density, ρ, and Poisson's ratio, ν (Krautkrämer, J. and Krautkrämer, H., 1990):

$$V_p = \sqrt{\frac{E(1-\nu)}{\rho(1+\nu)(1-2\nu)}} \quad (1)$$

The S-wave propagates at a slower speed, V_s is a function of the shear modulus of elasticity, *G*, and density, ρ:

$$V_s = \sqrt{\frac{G}{\rho}} = \sqrt{\frac{E}{\rho 2(1+\nu)}} \quad (2)$$

The ratio (α) of S-wave speed to P-wave speed is determined by equation (3). For a Poisson's ratio of 0.2, which is typical of concrete, α is 0.62. The ratio of the R-wave speed, V_r, to the S-wave speed is given by equation (4).

$$\alpha = \frac{Vs}{Vp} = \sqrt{\frac{(1-2\nu)}{2(1-\nu)}} \tag{3}$$

$$\frac{Vr}{Vs} = \frac{0.87+1.12\nu}{1+\nu} \tag{4}$$

For Poisson's ratio of 0.2, the R-wave speed is 92% of the S-wave speed, or 56% of the P-wave speed.

1.1.3 Reflection and Refraction. When a P-wave or S-wave front is incident on a boundary between dissimilar materials, a portion of stress-waves are reflected (Figure 1.2). The remainder penetrates into the underlying material (wave refraction) (Krautkrämer, J. and Krautkrämer, H., 1990).

The angle of refraction β, is a function of the angle of incidence θ, and the ratio of wave speeds, C_2/C_1, and is given by Snell's law (Malhotra and Carino, 2004):

$$\frac{\sin\theta}{C_1} = \frac{\sin\beta}{C_2} \tag{5}$$

The amplitude of the reflection is a function of the angle of incidence and is a maximum when this angle is 90° (normal incidence). For normal incidence the reflection coefficient, R, is given by the following equation:

$$R = \frac{Z_2 - Z_1}{Z_2 + Z_1} \tag{6}$$

where

Z_2 = specific acoustic impedance of material 2

Z_1 = specific acoustic impedance of material 1

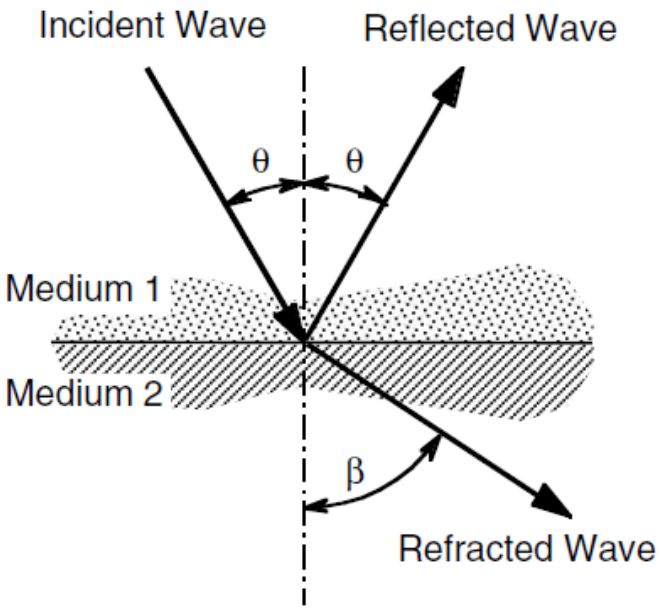

Figure 1.2 The Behavior of a P-wave Incident on an Interface between Two Dissimilar Materials: Reflection and Refraction (adapted from Malhotra and Carino, 2004)

The specific acoustic impedance is the wave speed and density of the material. The following Table 1.1 are summarized approximate values of the specific acoustic impedance for some typical materials.

When a stress wave traveling through concrete-air interface, there is almost total reflection at the interface. This is the cause of the stress-wave based methods have proven to be successful for locating defects within solids.

Table 1.1 The Specific Acoustic Impedance Values for some Typical Materials (adapted from Sansalone and Carino, 1991)

Material	Specific acoustic impedance, kg/(m^2s)
Air	0.4
Soil	0.3 to 0.4 x 10^6
Water	0.5 x 10^6
Concrete	7 to 10 x 10^6
Steel	47 x 10^6

The reflection coefficient (R) given by equation (6) can be negative or positive depending on the relative values of the acoustic impedances of the two materials (Malhotra and Carino, 2004). If Z_1 is greater than Z_2, such as the concrete-air interface, R is negative, indicating that the reflected wave will have the opposite sign, that is, a phase occurs. This means that the stress changes sign. For example, if the stress in an incident P-wave is compressive, the stress in the reflected P-wave is tensile. If Z_2 is greater than Z_1, no phase change occurs. These differences are critical for distinguishing between reflection from a concrete-air interface and from a concrete-steel interface.

1.2 ULTRASONIC SURFACE WAVE (USW)

The USW method is used to estimate material properties (velocity of propagation of surface waves or in-situ elastic modulus) of a medium (Baker *et al.*, 1995). The frequency range of interest is limited to a high-frequency range where the surface wave's penetration depth is less than the thickness of the tested object. The USW method is

based on impacting the surface of the tested object and recording the response of the object with at least two transducers. Signal and spectral analyses are used to create the phase of cross power spectrum and the coherence function between the two transducers (Baker *et al.*, 1997). The variation of Rayleigh wave phase velocity with wavelength shorter than slab thickness is measured from the phase of cross power spectrum to generate a dispersion curve. Then the average Young's modulus (dynamic elastic modulus) of the material can be calculated based on the following equation with an assumed or measured density and Poisson's ratio:

$$E = 2\rho[(1.13-0.16\nu)V_R]^2(1+\nu) \quad (7)$$

where:

V_R = phase velocity of surface wave,

ρ = density

ν = Poisson's ratio

In the case of a uniform or intact medium, the dispersion curve shows a relatively constant phase velocity with wavelength less than thickness of the tested object. In the case of the medium contained the deterioration, the average phase velocity becomes less than that of an intact medium, and the velocity obtained may be called an apparent velocity.

1.3 IMPACT-ECHO (IE)

The impact echo method is commonly used to detect flaws in concrete members as well as measure the thickness of tested object (Sansalone, 1997). The IE method is based on striking the concrete surface with an impactor, generating and transmitting

stress waves at frequencies of up to 20 to 30 kHz and measuring the response by a nearby receiver. The recorded time-domain signal is converted into a frequency-domain (amplitude spectrum) signal with the fast Fourier transform (FFT) analysis method. Then, the frequency of reflection, named "return frequency" is monitored. In the case of an intact concrete slab, the return frequency (f, also known as the thickness frequency) along with the measured or estimated compressional wave velocity Vp, can be used to estimate the slab thickness h with the following equation:

$$h = \beta\frac{V_P}{2f} \tag{8}$$

where:

$\beta = 0.96$ for concrete plates

V_P = compressional wave velocity

f = thickness frequency

h = slab thickness

The compressional wave velocity of concrete can be estimated based on the measured surface wave phase velocity with an assumed Poisson's ratio value:

$$V_P = (1.13\text{-}0.16\nu)V_R\sqrt{\frac{1-\nu}{0.5-\nu}} \tag{9}$$

where:

V_P = compressional wave velocity

V_R = Surface wave phase velocity

ν = Poisson's ratio

Other reflectors could be voids, delaminations or various types of defects with different acoustic impedance than that of concrete. In the case of a deep delaminated area,

the return frequency shifts to higher values than the thickness frequency. A wide or shallow delaminated area is generally dominated by a peak frequency much less than the thickness frequency, indicating that a flexural-mode vibration dominates the frequency response. In this case, the slab thickness and the depth of the delamination cannot be calculated on the basis of equation (8).

1.4 PORTABLE SEISMIC PROPERTY ANALYZER (PSPA)

All experimental tests were carry out with a portable seismic property analyzer (PSPA) in this study. As shown in Figure 1.3, the PSPA consists of two vertical transducers and a solenoid-type source packaged into a handheld portable system that can perform the USW and IE tests simultaneously. The device is connected to a laptop computer that controls the PSPA and automatically stores and interprets the acoustic signals recorded by the transducers. The impact duration is approximately 130 μs and the data acquisition system has a sampling frequency of 390 kHz per channel. Each measurement took approximately 30 seconds in the field.

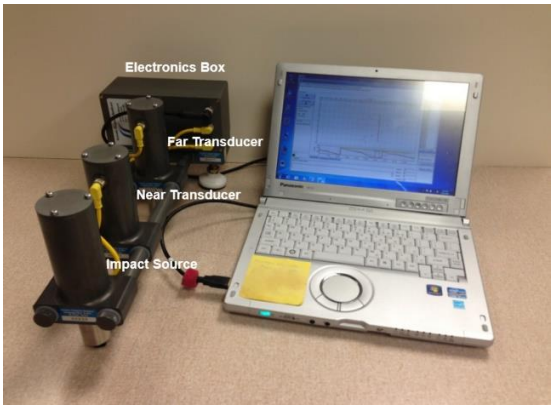

Figure 1.3 Portable Seismic Property Analyzer (PSPA)

1.5 COMMON TYPE OF DEFECTS IN CONCRETE BRIDGE DECKS

The deterioration of steel-reinforced concrete bridge decks can be caused by many reasons, such as poor initial quality, damage from deicing slats, overloading, free-thaw cycle, fatigue and corrosion of rebar (Gucunski *et al.*, 2013). Among all the deterioration phenomena listed above, three deterioration mechanism are of the highest concern to transportation agencies: a) Rebar corrosion; b) Deck delamination; and c) Concrete degradation. Each of the deterioration mechanism is briefly discussed in the following sections.

1.5.1 Rebar Corrosion. Chlorides are derived primarily from the application of roadway deicing slats, is a major contributor to the problem of rebar corrosion. The oxide film, which is used to protect the corrosion of reinforcement steels embedded in concrete bridge decks, can be destroyed by chloride diffusion, which is induced the electro-chemical process or corrosion begins. Corrosion of steel reinforcement in a concrete bridge deck can directly reduce the structural capacity of the deck. Furthermore, the corrosion process can cause internal stress, cracking, delamination and eventually spalling to the concrete surface.

1.5.2 Deck Delamination. Delamination or horizontal cracking induced by corrosion of embedded reinforcing steel is the major and serious form of deterioration in concrete bridge decks. The expansion of reinforcing steel as it corrodes can create a crack or subsurface fracture plane in the concrete. Delamination is not visible on the concrete surface; however, if repairs are not made in a timely fashion, the delamination progresses to open spalls and eventually affect the structural integrity of the deck.

1.5.3 Concrete Degradation. A reduction of concrete strength or modulus is considered to be a form of concrete degradation. Many physical or chemical phenomena can induce the concrete degradation, such as the micro-cracking, alkali-silica reaction (ASR), plastic shrinking, and freeze-thaw cycles. The ASR is a reaction between reactive silica phases in aggregates and alkali hydroxides in the concrete pore solution. This reaction produces a silica gel that swells in the presence of water, causing internal and external cracking; plastic shrinkage can cause cracks in concrete. These cracks often occur on plane structures such as deck slabs; Freeze-thaw cycles can increase the hydraulic pressure in concrete. The concrete will rupture once the pressure exceeds the tensile strength of the concrete, and cause extensive deterioration in the form of cracking, scaling, and crumbling.

1.6 COMMON TYPE OF DEFECTS IN CONCRETE PAVEMENTS

The deterioration of cement concrete pavement can be caused by many reasons, such as overloading, free-thaw cycle, fatigue, shrinkage and damage from deicing slats. Common types of distresses in concrete pavements are a) Cracking b) Joint distress c) Surface distress and d) Overlay debonding (Johanns and Craig, 2002). Each of the deterioration mechanism is briefly discussed in the following sections.

1.6.1 Cracking. Cracking is the most common type of defects in concrete pavement, such as the longitudinal cracking, transverse cracking, durability cracking (“D” cracking), slab cracking, pattern cracking and corner breaks. Many factors can induce cracking in concrete pavement, such as overloading, settlement of subgrade material, long joint-spacing, plastic shrinkage and freeze-thaw cycles. If repairs are not made, the

moisture with other fine materials can enter the pavement through those cracks, accelerating the deterioration progress of concrete and subgrade material to other serious problems, such as the scaling and pumping, and eventually affect the structural integrity of the pavement.

1.6.2 Joint Distress. Joint distresses occur at various spacing on jointed concrete pavement and can cause an unpleasant ride if not properly maintained. Joint failures appear in many forms from minor to major, such as the transverse joint cracks, open spalling, faulting and pumping. Many factors can induce the joint distress in concrete pavement, such as the expansive internal pressure due to corrosion of dowel bars or ASR reactions between cement and aggregates, thermal expansion due to freeze-thaw cycles, overloading and lack of support at joint due to pumping action and voids. If repairs are not made, the deterioration progress to loss the support of subgrade material and eventually affects the structural integrity and safety of the pavement.

1.6.3 Surface Distress. Surface distress is the scaling, spalling, polished aggregate, popouts and disintegration of the concrete wearing surface that leads to roughness and poor durability. Several factors can induce the surface distress in concrete pavement, such as the poor initial construction, thermal and moisture stresses and corrosion of reinforcing steel too close to pavement surface. The surface distress can cause an unpleasant ride if not properly maintained.

1.6.4 Overlay Debonding. Parts of old concrete pavement is overlaid with asphalt concrete (AC) or portland cement concrete (PCC). The overlay can debond from the existing concrete pavements. Once an overlay debond, moisture and chlorides may enter the debonded region, further promoting deterioration. If repairs are not made,

debonded overlay region can eventually deteriorate into open spalls, which affect the ride quality and the structural integrity of the pavement. In addition, bonded and debonded overlays contribute to the complexity of the analysis of NDT methods and may impede their effectiveness.

PAPER

I. Application of ultrasonic surface wave techniques for concrete bridge deck condition assessment

Mengxing Li *
Department of Geological Engineering, Missouri University of Science and Technology, Rolla MO 65409, USA, Email: mlzg9@mst.edu

Neil Anderson
Department of Geological Engineering, Missouri University of Science and Technology, Rolla MO 65409, USA, Email: nanders@mst.edu

Lesley Sneed
Department of Civil, Architectural and Environmental Engineering, Missouri University of Science and Technology, Rolla MO 65409, USA, Email: sneedlh@mst.edu

Norbert Maerz
Department of Geological Engineering, Missouri University of Science and Technology, Rolla MO 65409, USA, Email: norbert@mst.edu

ABSTRACT

Ultrasonic surface wave (USW) is a well-established technique for the performance monitoring of concrete structures. In order to investigate the capability and reliability of this technique for concrete bridge deck condition assessment, a portable seismic property analyzer (PSPA) with USW capabilities was used to assess the condition of a reinforced concrete bridge deck exhibiting visible evidence of significant deterioration. After the investigation was completed, variable thicknesses of concrete were removed from upper surface of the concrete deck by milling and hydrodemolition, with greater thickness being removed where the concrete was more deteriorated. The thickness of removed concrete during the hydrodemolition process was mapped by Light Detection and Ranging (LiDAR). A comparison of the thickness of concrete removed and the USW data indicates that there is a qualitative correlation between the USW results at each test location and the thickness of concrete removed at those same test locations.

Results suggest that the PSPA, and comparable USW techniques, could be potentially effective for estimating the thicknesses of concrete that would be removed during milling and hydrodemolition, although more work is needed to study the relationship between USW and removal thickness data in order to be used for quantity estimations.

Key words: concrete bridge deck, hydrodemolition, light detection and ranging, portable seismic property analyzer, ultrasonic surface wave

1. Introduction

Milling, followed by hydrodemolition, is commonly used to remove the upper surface of concrete bridge decks during rehabilitation (ICRI, 2004a). The expectation is that greater thickness of concrete will be removed where the concrete is in poor condition; less thickness will be removed where the concrete is in good condition. One of the technical challenges facing those engaged in budgeting for bridge deck repairs is estimating the volume of concrete that will be removed by hydrodemolition.

Ultrasonic surface wave (USW) is a well-known non-destructive testing technique commonly used for determining the condition and properties of concrete structures (McDaniel *et al.*, 2010; Azari *et al.*, 2014). A recent study conducted by Azari *et al.* (2012) on a constructed concrete bridge deck demonstrated that the USW method proved effective to locate and characterize shallow defective areas (3 in. deep) in the deck. In addition, test density and configuration has also been found to impact the accuracy of USW test results (Azari *et al.*, 2012).

In this investigation, USW data were acquired using a portable seismic property analyzer (PSPA) at multiple predetermined locations across a concrete bridge deck prior to milling and hydrodemolition (Fig. 1). The PSPA-USW data acquired at each test

location were used to generate a 1-D plot of elastic modulus (Young's modulus) versus depth (Gucunski *et al.*, 2008). The 1-D elastic modulus plots extended from a depth of 2 in. to a depth of approximately 7.5 in. Nine cores retrieved from the concrete deck (before deck rehabilitation) were used to assess the PSPA-USW test results.

Fig. 1. Photo of the bridge.

After the PSPA-USW investigation was completed, the bridge deck was rehabilitated by milling followed by hydrodemolition. Hydrodemolition involves the use of high pressure water jets to remove the uppermost layer of concrete.

Light Detection and Ranging (LiDAR) was used to map the deck surface both before and after the process of milling and hydrodemolition in order to calculate the

spatial distribution of the thicknesses of concrete removed from the bridge deck surface. The LiDAR measured thickness of concrete removed at each PSPA test location was compared with the corresponding 1-D elastic modulus data to determine if there was statistical correlation between the PSPA-USW and hydrodemolition results.

The objective of this study was to determine if there is a statistical correlation between the PSPA-USW elastic modulus and hydrodemolition data, which would imply that the PSPA tool could potentially be used to estimate the relative thickness of concrete that would be removed during deck rehabilitation. The effectiveness and limitations of the PSPA-USW method are also assessed and summarized in this paper.

2. Background information

2.1. PSPA

The PSPA is an ultrasonic acoustic tool that measures the phase velocities of Rayleigh waves at discrete test locations (Fig. 2). The PSPA tool automatically transforms the phase velocity data acquired at each test location into a 1-D plot of elastic modulus (Young's modulus). In this study, the elastic modulus of the concrete was measured over the depth range of 2 in. to ~7.5 in. due to the limitations of sensor spacing as well as the range of analysis frequencies provided by PSPA: 0-50000 Hz. The authors considered this to be a potential source of error since milling and hydrodemolition removed less than 2 in. of concrete across about 85% of the bridge deck.

Generally, it is easier to obtain the value of the Rayleigh wave velocity than the P-wave (compressional wave) velocity in the field. The authors have analyzed full waveform PSPA data acquired during the course of this investigation (and during previous investigations) and concluded that first arrival times cannot be identified or

measured, presumably because the receiver transducers are vertically polarized. In fact, it is very challenging to identify first arrival time of P-waves in waveform records due to the strong background noise generated from various sources in the field (e.g., traffic).

Fig. 2. Portable seismic property analyzer (PSPA).

The PSPA tool calculates the elastic modulus E (Young's modulus) of the concrete based on the relationship described in Equation 1 (Baker *et al.*, 1995):

$$E= 2\rho[(1.13-0.16\nu)V_R]^2(1+\nu) \quad (1)$$

where:

V_R = measured Rayleigh wave velocity

ρ = density

ν = Poisson's ratio

Values of density (150 pcf) and Poisson's ratio (0.18) for "good quality concrete" as defined by the PSPA software (PSPA Manager) were employed in this study. Based on Equation 1, it should be noted that the value of Poisson's ratio is not significant compared the value with V_R in the calculation of E, for example, increasing Poisson's ratio from 0.2 to 0.3 with the same values of density and V_R increases the value of E by 5%. Therefore, the measured value of V_R is the dominant factor in the calculation of E.

The PSPA software also calculates the average elastic modulus (E_{avg}) of the bridge deck over the depth range tested (2 in. to ~7.5 in.). It should be noted that if the section of bridge deck tested is comprised of different materials with different acoustic properties (an asphalt patch on a concrete deck, for example), the calculated value of E_{avg} will not accurately represent the average modulus since the value of density and Poisson's ratio are defined for a single material. Rather it represents an apparent average elastic modulus over the entire depth range tested.

According to the reference Table 1, good quality concrete is characterized by elastic modulus values greater than 4500 ksi, and poor quality concrete is characterized by elastic modulus values less than 4000 ksi (McDaniel *et al.*, 2010).

Table 1
Typical values of elastic modulus for concrete bridge decks (adapted from McDaniel et al., 2010).

Concrete quality	Good	Fair	Poor	Severe
Concrete elastic modulus (ksi)	≥ 4500	4000 - 4500	3500 - 4000	≤ 3500

2.2. Hydrodemolition

Hydrodemolition is a process that utilizes high-pressure water to mechanically remove unsound concrete from bridge decks and has been widely used in the rehabilitation of concrete bridge decks (ICRI, 2004a). The material removed by the hydrodemolition process generally has lower strength than the sound concrete that is left in place. The expectation is that greater thickness of concrete will be removed where the concrete is in poor condition; whereas, lesser thickness will be removed where the concrete is in good condition.

In this study, the concrete bridge deck was rehabilitated by a process that involved milling of the surface followed by hydrodemolition to remove unsound material. Prior to hydrodemolition, the top 0.25 in. of concrete was to be removed by the milling process. Milling the concrete left behind a rough and grooved surface as shown in Fig. 3.

After the milling process was complete, a hydrodemolition machine with high water pressure jets (14200 psi) was calibrated to remove a minimum of 0.5 in. of concrete from the entire bridge deck surface (Fig. 4). Milling and hydrodemolition was expected to remove at least 0.75 in. of concrete from the entire bridge deck surface. In reality however, LiDAR results indicate that less than 0.75 in. of concrete was removed from 58% of the bridge deck surface area. The minimum thickness of concrete removed at any

location on the bridge deck was 0.012 in.; elsewhere reinforcing steel at a depth of 2 in. (to top of reinforcing steel bars) was completely exposed.

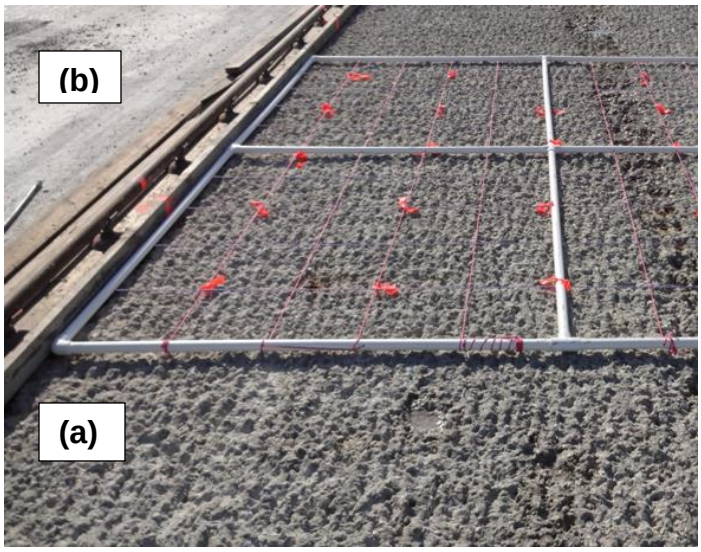

Fig. 3. Rough, grooved concrete surface caused by milling (a) and original as built concrete surface (b).

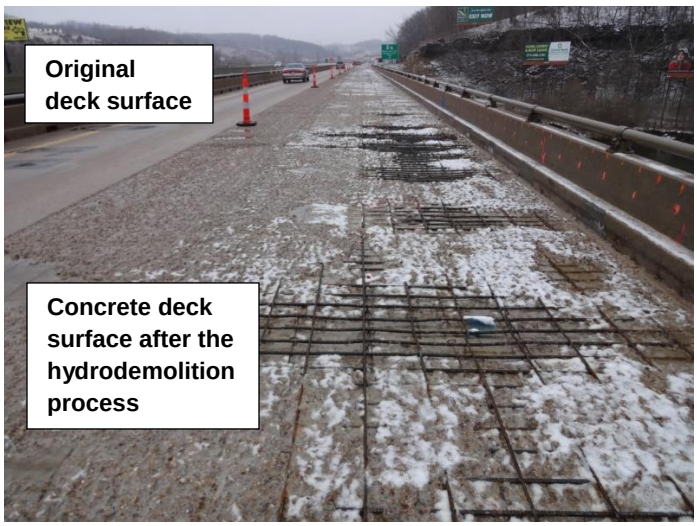

Fig. 4. Photo of the bridge deck surface after hydrodemolition process.

2.3. LiDAR

In this study, LiDAR was employed to map the deck surface before and after hydrodemolition in order to estimate the thickness of the concrete removed from the deck during the hydrodemolition process. Fig. 5 demonstrates the LiDAR scanner set up to scan the bridge deck after hydrodemolition. Two LiDAR scans were performed on the bridge deck undergoing rehabilitation process. The first scan was completed less than a week before the milling of the concrete bridge deck took place. The second scan was conducted after completion of the concrete removal by milling and hydrodemolition process but prior to placing the new concrete overlay. The location and thickness of removed concrete across the bridge deck was determined by subtracting the pre-rehabilitation LiDAR data from the post-hydrodemolition data. Fig. 6 demonstrates a typical segment (85 ft length) image generated by subtracting the second scan from the first scan. The embedded reinforcing steel is visible in the figure, along with the rough surface created by the milling of the deck surface.

The accuracy of the LiDAR measurements for each segment (13 x 85 ft) varied from 0.08 in. to 0.24 in. Measurements were taken from the scanner mounted in a fixed location with a vertical sweep angle varying from 0-40 degrees (see Fig 5). At near range, the LiDAR beam is more orthogonal to the scanned surface, but at far range, the beam hits the surface at a very shallow angle. This low (shallow) scan angle makes it difficult to image zones with an abrupt change in thickness. This could be a source of error that affects the LiDAR accuracy.

It should be noted that most of the PSPA study areas (discussed in Section 3.2) were either located in the middle or near sections of the LiDAR segments (only part of

area A was located in the far end of one LiDAR segment). Therefore, the error of the LiDAR measurements acquired in the PSPA study areas should be much lower than 0.24 in.

Fig. 5. LiDAR scanner set up to scan the bridge deck after hydrodemolition was used to remove unsound concrete.

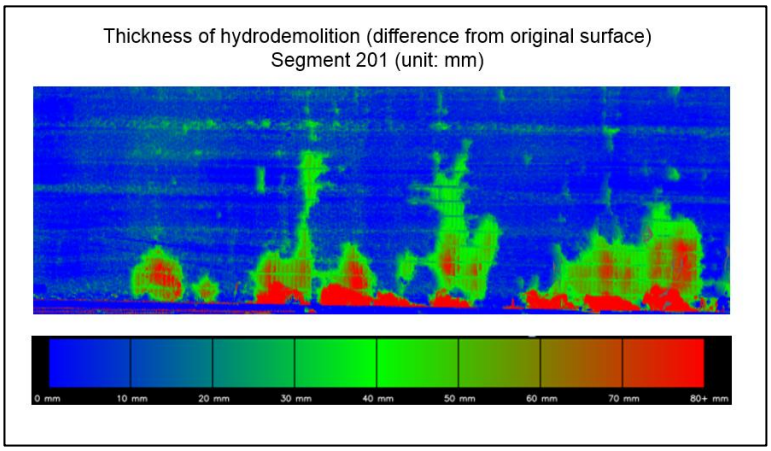

Fig. 6. LiDAR image of the bridge deck showing thickness difference between pre-rehabilitation and post-hydrodemolition.

3. Case study description

3.1. Description of the bridge deck

The two-lane test bridge was constructed in 1966 and is located in central Missouri. The main structure of the bridge is a continuous steel girder system that consists of five spans. The bridge deck is a solid cast-in-place concrete slab that is 868 ft long, 32 ft wide, and 7.5 in. thick. Fig. 7 shows a longitudinal and transverse cross section of the bridge deck. The deck is reinforced with two mats (two orthogonal layers per mat) of steel reinforcing bars spaced at 6.0 in. in the bridge transverse direction (perpendicular to traffic) and spaced 6 in. to 12 in. in the bridge longitudinal direction (parallel to traffic). The depths of the upper and lower mats of reinforcing steel are 2 in. and 5 in. (clear) from the deck top surface, respectively. Asphalt and concrete patches were present in places.

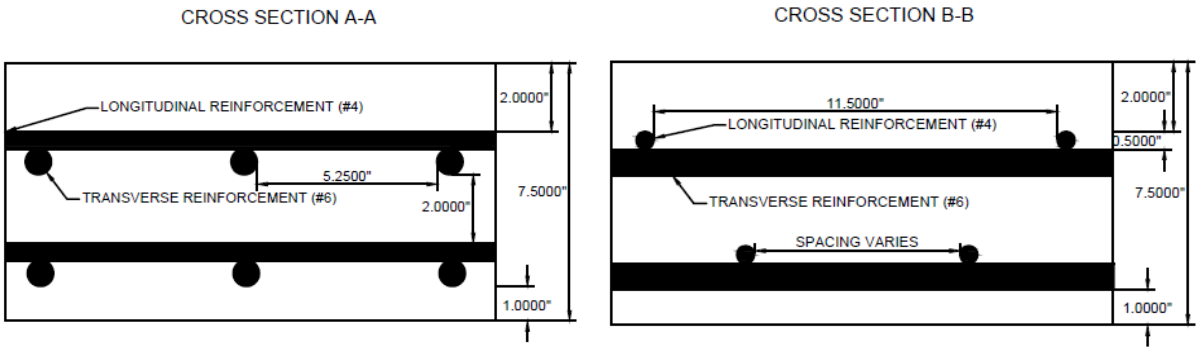

Fig. 7. Longitudinal (AA') and transverse (BB') cross sections of the bridge deck showing reinforcement details.

3.2. Test plan and data collection

A total of 161 defects were documented during a comprehensive visual inspection of the entire bridge deck. Documented defects included concrete patches, unfilled concrete potholes, asphalt patches, and transverse cracks. Based on the visible evidence, the deck surface appeared heavily deteriorated near the middle of the beam spans. Deterioration levels appeared to be much lower near the bent supports.

Nine 2 in. diameter cores were retrieved from the top surface of the deck (before deck rehabilitation) at locations determined on the basis of the visual inspection results. Core locations are shown in Fig. 8 and were selected both from areas where the bridge deck visually appeared to be in good condition and areas where the deck visually appeared to be degraded or to have been previously repaired. The results of core conditions were used to assess and verify the PSPA-USW test results.

A total of 120 PSPA-USW test points was obtained in this study, and all field work was completed in 6 hours with a two-person crew. Based on consideration of time and traffic control cost, six areas (4 ft x 10 ft) were selected randomly as the PSPA test locations shown in Fig. 8. Some of the PSPA-USW test points were located on asphalt and concrete patches, especially in the test areas where significant visible evidence of deterioration was present. PSPA-USW data were also acquired at all core locations before the cores were extracted.

Prior to the PSPA-USW tests, a ground-coupled ground penetrating radar (GPR) system with high frequency antenna (1.5 GHz) was utilized in the PSPA-USW test areas in order to image the locations of the upper mat of the reinforcing steel. Then, the PSPA instrument was placed in the center of the upper mat of the reinforcement steel at each

test location as shown in Fig. 9. According to previous research conducted (Aggelis and Shiotani, 2007; Malhotra and Carino, 2004), the propagation of surface waves is insensitive to the presence of reinforcing steel if the diameter of the reinforcement steel is much smaller than the size of the test grid and minimum detectable wavelength. In this study, the diameter of the reinforcement steel bars (0.5 in. and 0.75 in. for the #4 and #6 bars, respectively) is much smaller than the size of the test grid (2x2 ft), as well as the minimum detectable wavelength of the PSPA-USW instrument (2 in.). Therefore, considering the remarks above and the placement of the PSPA instrument, the influence of the reinforcing steel on the PSPA-USW test results should be negligible.

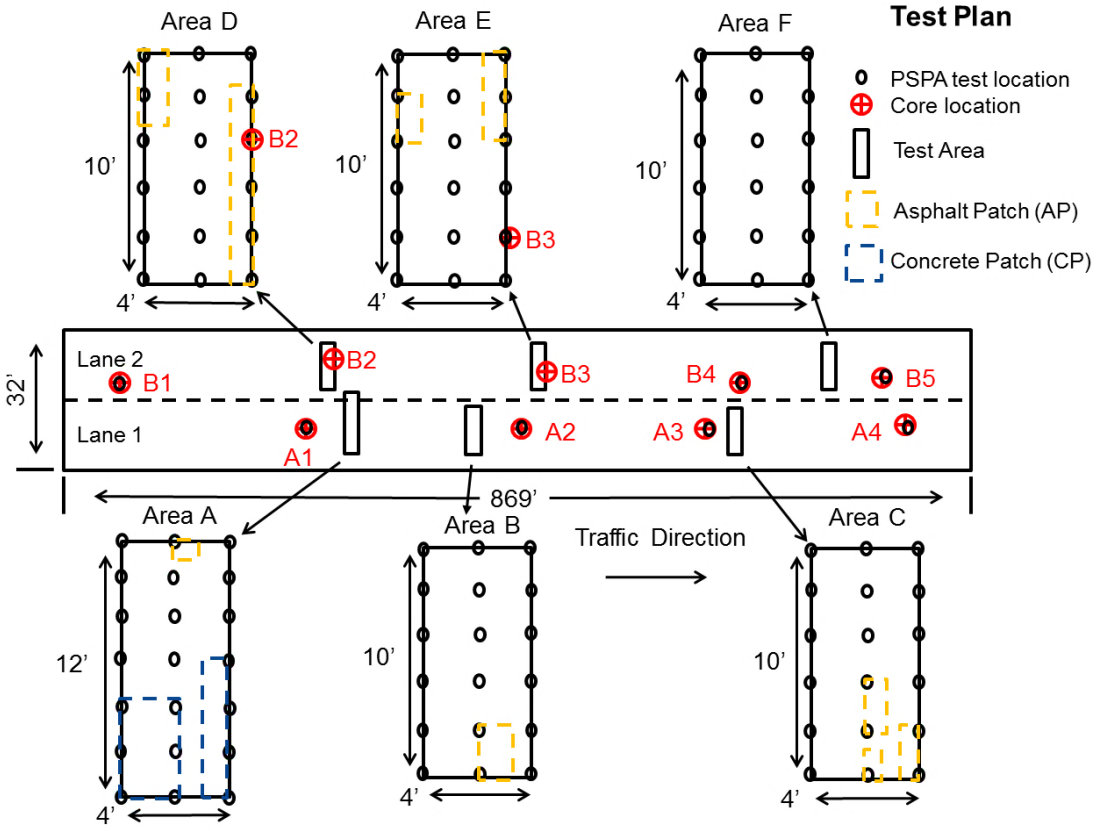

Fig. 8. Test plan showing the PSPA test and core locations on the bridge deck.

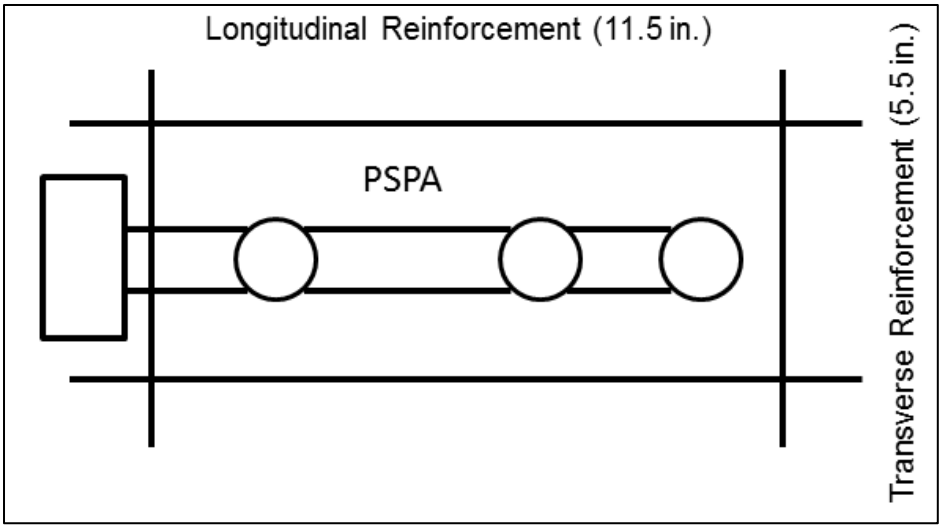

Fig. 9. Sketch of the test location of the instrument (PSPA) on deck surface.

It should be noted that 16 of the 120 PSPA-USW test points were acquired on asphalt patches. Accordingly, the calculated elastic modulus of the concrete at locations of asphalt patch locations may be underestimated where the asphalt patch thickness is more than 2 in. since average elastic modulus values are not indicative of the strength of the asphalt patch.

4. Core results

The cores were carefully examined and documented in terms of material, number of pieces and the length of each piece, visible voids, presents of delaminations, segregation of the aggregate, and presence of cracks. Based on these properties, the cores were then given a visual core rating defined for this project of either “Good”, “Fair”, “Poor”, or “Severe” (Fig. 10). In this study, a visual core rating of “Good” indicates that the core had no delamination or visible deterioration present. “Fair” indicates that the core had some visible minor deterioration including cracks and voids, however the

concrete was in one piece. “Poor” indicates that the core had some major deterioration including delaminations, however the concrete was in a few large sections. “Severe” indicates that the core had a lot of deterioration and was in many pieces when extracted, including several small pieces. Visual core ratings are summarized in Table 2.

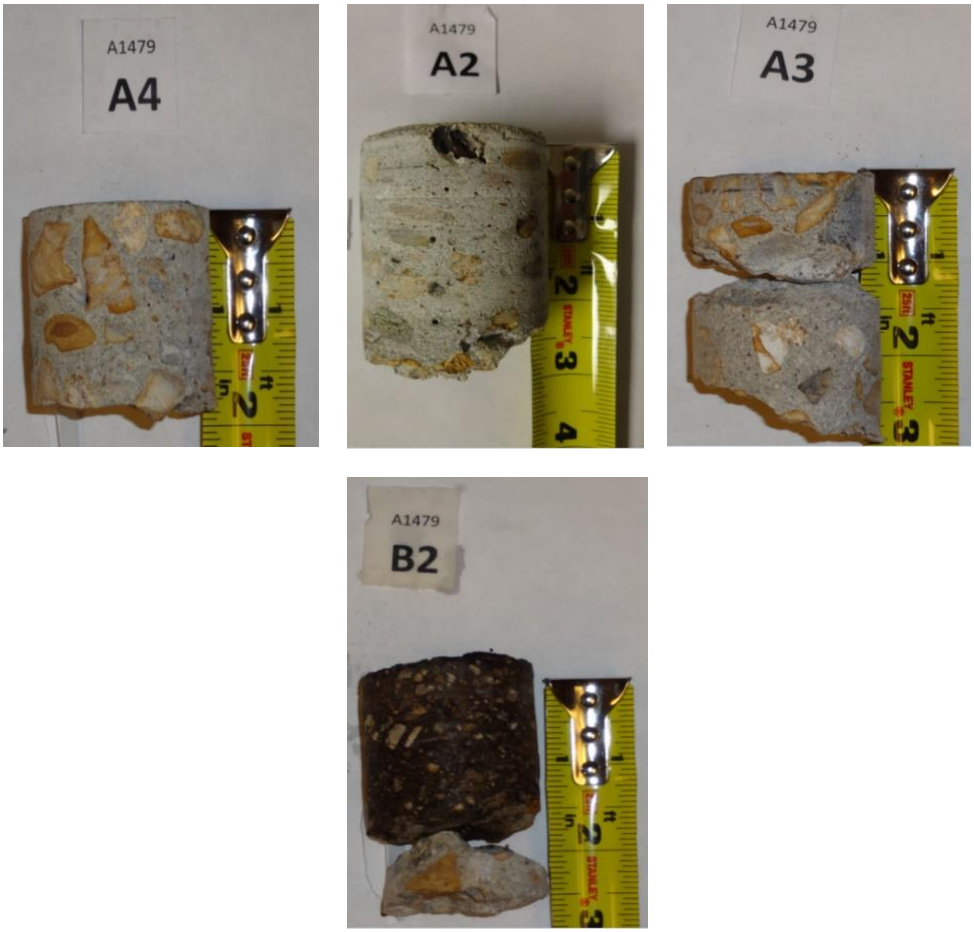

Fig. 10. Photos of representative core samples with different core conditions. Core A4 (good): no visible delamination or deterioration; core A2 (fair): cracks observed at a depth of 1 in.; core A3 (poor): delaminations observed at a depth of 1 in.; core B2 (severe): delaminations observed at a depth of 2.5 in., and debonded asphalt patch observed at a depth of 2 in.

5. PSPA-USW data presentation and analysis

The elastic modulus was calculated at each PSPA test point using the default values of density (150 pcf) and Poisson's ratio (0.18) defined for good quality concrete. 1-D plots of elastic modulus vs. depth were generated at each test point location for the depth range tested (2 in. to ~7.5 in.). The PSPA software was also used to calculate the average elastic modulus over the depth range tested at each test point. The average elastic modulus values were converted into 2-D contour plots showing the surface distribution of average modulus for each of the six test areas (Fig. 8).

Table 2
Average elastic modulus of the bridge deck in immediate proximity to each core location (within 6 in.).

Core number	Average measured elastic modulus (ksi)	Core condition
A1	3243	Poor (concrete delaminated at depth of 1 in.)
A2	4095	Fair (visible cracks)
A3	2720	Poor (concrete delaminated at depth of 1 in.)
A4	4470	Good (no visible evidence of deterioration)
B1	4866	Good
B2	1486	Severe (asphalt was debonded at depth of 2 in.; concrete delaminated at depth of 2.5 in.)
B3	4844	Fair (visible cracks at depths of 1 in. and 2 in.)
B4	4450	Poor (concrete delaminated at depth of 1.75 in.)
B5	4817	Good

The elastic modulus values at the core locations are presented and compared with core assessments in Section 5.1. The elastic modulus values in the six test areas are presented and compared with the LiDAR survey of the thickness of concrete removed during hydrodemolition in Section 5.2.

5.1. Comparison of PSPA-USW and core results

Representative PSPA-USW test results at the core locations are shown in Fig. 11 in terms of elastic modulus vs. depth. The PSPA-USW data shown in Fig. 11 were collected at test points in immediate proximity to the core locations as discussed in Section 3.2. Core conditions are described in Section 4.

Core B2 (shown in Fig. 10) was retrieved from an asphalt patch location. According to core results (Table 2), the interface between the asphalt and concrete was debonded at the depth of 2 in., and the concrete was delaminated at the depth of 2.5 in. The elastic modulus values obtained in immediate proximity to core B2 decrease slightly with depth from 2 in. to 7 in. The average value of elastic modulus is 1486 ksi, which is significantly lower than the value corresponding to severe quality concrete (Table 1). The values of modulus in Table 1 were calculated based on concrete material, however, core B2 contained 2 in. of asphalt as well. Accordingly, the average value of elastic modulus should be an apparent value.

Core A3 (shown in Fig. 10) was retrieved from a location with no visible evidence of deterioration from the surface of the deck, although a delamination was noted at the depth of 1 in. upon inspection of the core hole (Table 2). The elastic modulus values obtained in immediate proximity to core A3 decrease with depth from 2 in. to 4 in.

The average value of elastic modulus is 2720 ksi, which is lower than the value corresponding to severe quality concrete (Table 1).

Core A2 (shown in Fig. 10) was retrieved from the concrete deck in an area with no visible evidence of deterioration (cracks at depth of 1 in.). The elastic modulus values obtained in immediate proximity to core A2 increase with depth from 2 in. to 4 in. then reduce from 4 in. to 7.5 in. The average value of elastic modulus is 4095 ksi, which is approaching the value associated with fair quality concrete (Table 1).

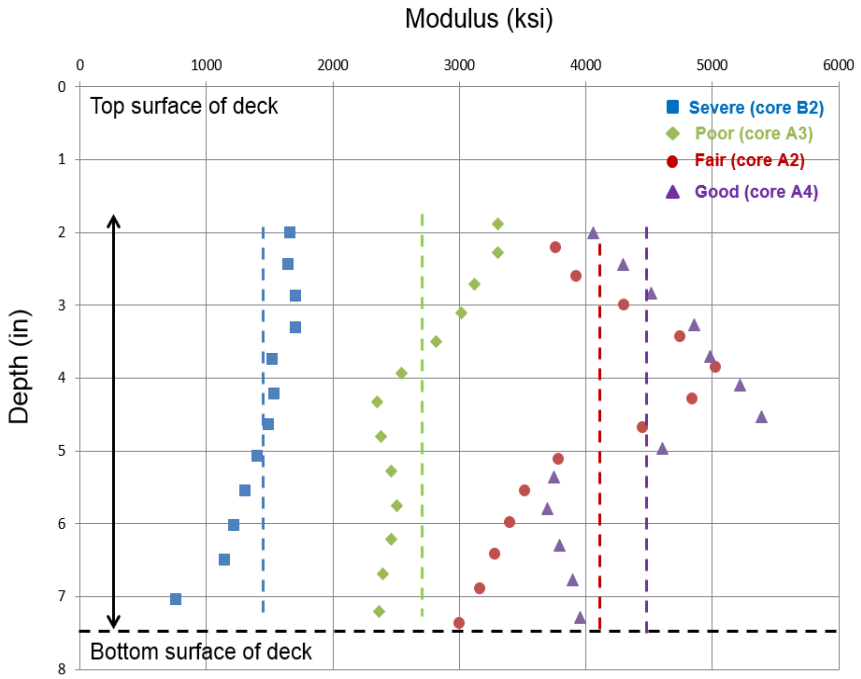

Fig. 11. Elastic modulus plots acquired in immediate proximity of core samples. Investigation depth is limited from ~2 in. to ~7.5 in. with 4 in. spacing between two transducers. The average elastic modulus for core samples with different core conditions: core B2 (Severe) = 1486 ksi; core A3 (Poor) = 2720 ksi; core A2 (Fair) = 4095 ksi; core A4 (Good) = 4470 ksi.

Core A4 (shown in Fig. 10) was retrieved from the concrete deck in an area with no visible evidence of deterioration. The elastic modulus values obtained in immediate proximity to core A4 increase with depth from 2 in. to 4.5 in. then reduce from 4.5 in. to 7.5 in. The average value of elastic modulus is 4470 ksi, which is approaching the value associated with good quality concrete (Table 1).

The average elastic modulus values (2 in. to 7.5 in.) and core conditions for each core sample are summarized and compared in Table 2. In general, test points with higher average elastic modulus values tend to have a better core rating, and test points with a lower average elastic modulus tend to have a poorer core rating. Core B4 is an exception with a poor core rating and high average elastic modulus, however, the deamination was noted to be above the depth range tested (~2 in. to ~7.5 in.). Therefore, the average modulus value at the Core B4 locations is representative of the concrete deck conditions from the depth of 2 in. to 7.5 in. Similarly, asphalt layer present in Core B2 was less than 2 in. thickness. The correlation between core results and the average elastic modulus suggested that the average elastic modulus (calculation over the depth of 2 in. – 7.5 in.) is indicative of the quality of the upper 2 in. of concrete.

In summary, a good qualitative correlation was observed between the PSPA-USW elastic modulus results and core condition assessment.

5.2. Comparison of PSPA-USW and hydrodemolition results

In this study, PSPA-USW data were acquired on a 2x2 ft test grid employed over different test areas (Fig. 8).

The USW data acquired at discrete points were converted to a 2-D contour plot. Representative 2-D contour plots of the average elastic modulus and the thickness of concrete removed during rehabilitation process are shown in Figs. 12 -14 for test areas D, B, and E, respectively, defined in Fig. 8.

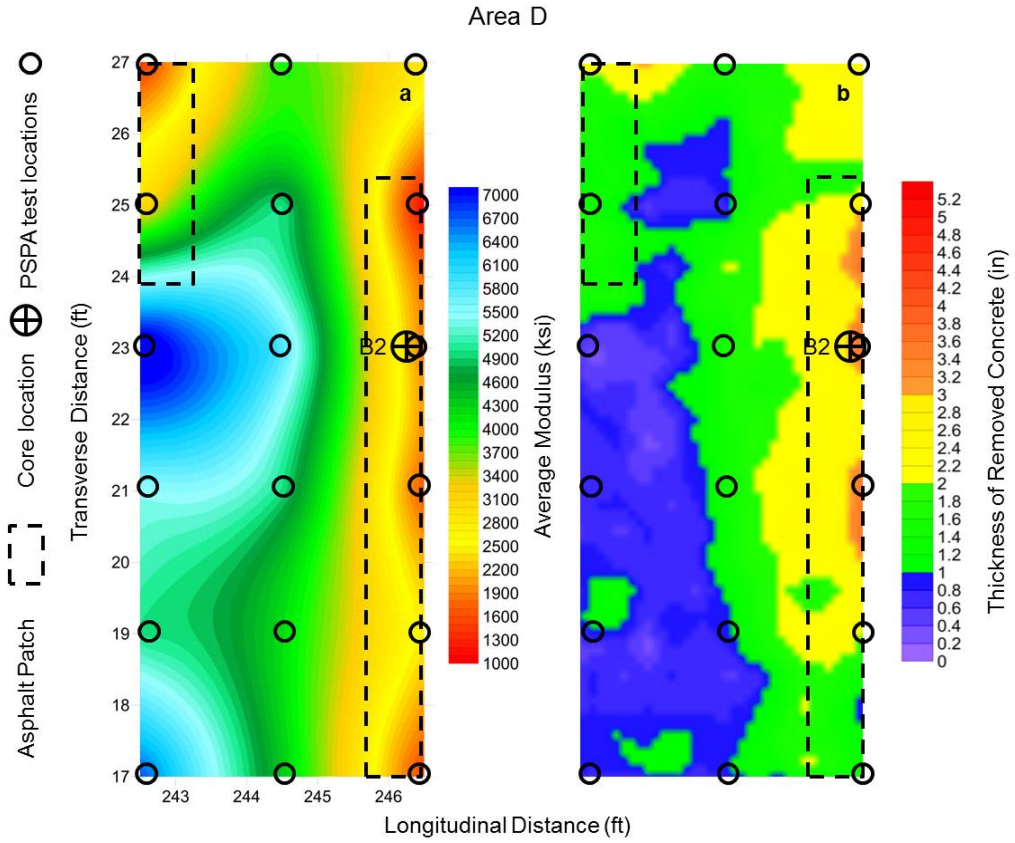

Fig. 12. 2-D contour plot comparison between the average modulus of concrete deck and the thickness of concrete removed during rehabilitation for area D (reference Fig. 8). The interval between each PSPA test point is 2 ft. The effective penetrating depth of PSPA-USW test range is from 2 in. to 7.5 in.

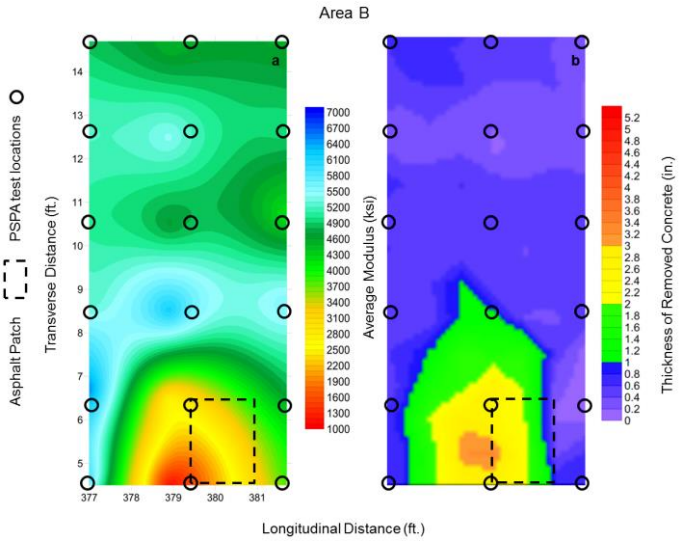

Fig. 13. 2-D contour plot comparison between the average modulus of concrete deck and the thickness of concrete removed during rehabilitation for area B (reference Fig. 8). The interval between each PSPA test point is 2 ft. The effective penetrating depth of PSPA-USW test range is from 2 in. to 7.5 in.

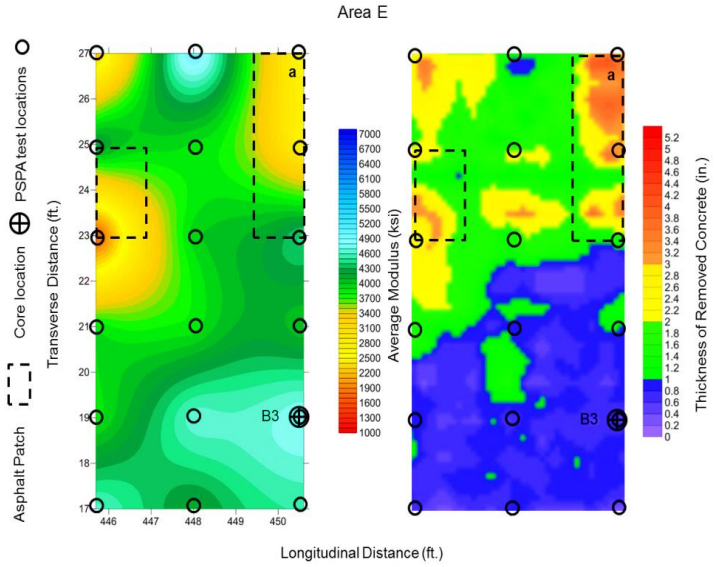

Fig. 14. 2-D contour plot comparison between the average modulus of concrete deck and the thickness of concrete removed during rehabilitation for area E (reference Fig. 8). The interval between each PSPA test point is 2 ft. The effective penetrating depth of PSPA-USW test rang is from 2 in. to 7.5 in.

Fig. 15 shows the distribution of the removed concrete thickness in terms of degradation level for the entire study area. Percentages of the entire study area with different concrete removal depth ranges (namely ≤ 0.75 in; 0.75 in. – 2 in.; ≥ 2 in.) were determined, and then the average elastic modulus of PSPA test points within the corresponding regions were averaged and compared. 47.5% of study area shows the evidence of low level of concrete degradation (removed concrete thickness ≤ 0.75 in.) with an average elastic modulus of 4775 ksi, which is consistent with good quality concrete on the basis of Table 1; 40.8% of study area shows the evidence of intermediate level of concrete degradation (0.75 in. ≤ removed concrete thickness ≤ 2 in.) with an average elastic modulus of 4242 ksi, which is consistent with fair quality concrete on the basis of Table 1;11.7% of study area shows the evidence of severe level of concrete degradation (removed concrete thickness ≥ 2 in.) with an average elastic modulus of 2829 ksi, which is consistent with severe quality concrete on the basis of Table 1. Overall, a good correlation can be identified between the average elastic modulus determined based on concrete removal depth ranges for the entire study area and the concrete quality determined from Table 1.

The relationship between the concrete removal depth and the average elastic modulus values for all PSPA test points (120) is shown in Fig. 16. In general, Fig. 16 shows that locations where greater thicknesses of concrete were removed are associated with lower values of average elastic modulus values. However, a significant amount of scatter in the data is also observed in Fig. 16.

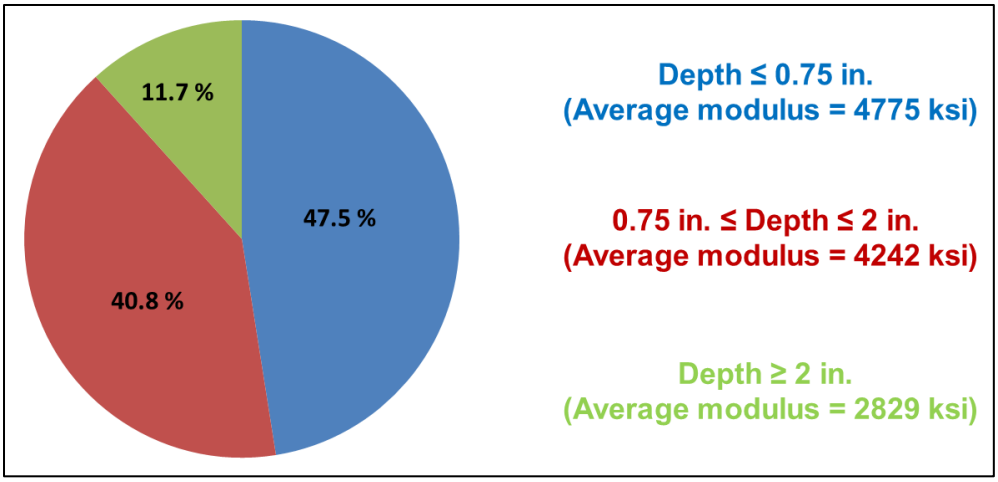

Fig. 15. Distribution of the removed concrete thickness for the entire study area.

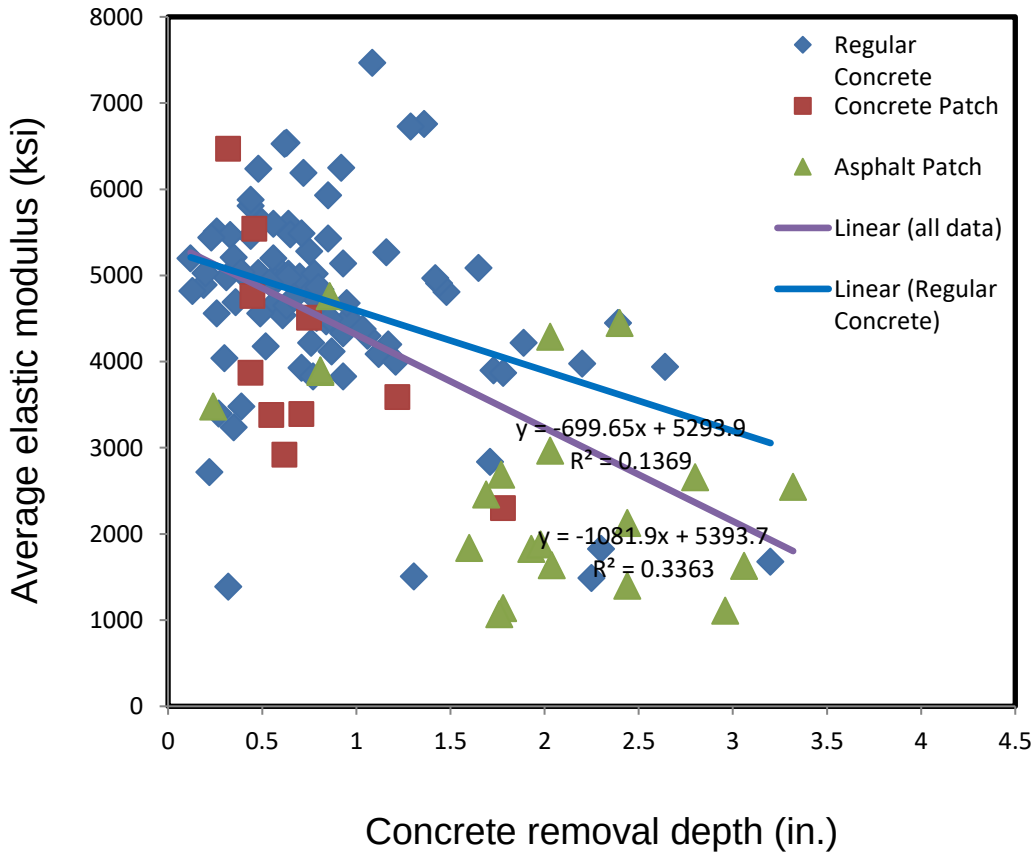

Fig. 16. Relationships between the average elastic modulus and the concrete removal depth values considering all PSPA data points and data points for regular concrete only.

As mentioned previously, the data collected at locations of asphalt patches represent average apparent elastic modulus values, not average elastic modulus values. The data points associated with locations of asphalt patches are identified in Fig. 16. As expected, most of the modulus values at locations of asphalt patches are relatively low, and they constitute many of the data points below the trend line (purple). Therefore, a corrected trend line was generated and plotted in Fig. 16 that excludes the data points associated with asphalt patches and also the concrete patches. The corrected trend line is less steep than initial trend line considering all test pints, and the scatter is also reduced.

However, the values of the correlation coefficients (R^2) demonstrated in Fig. 16 for both trendlines (0.14 for regular concrete and 0.34 for all data) are significantly low, which is an indication of poor correlations between the concrete removal depth and the average elastic modulus values obtained in this study. Several factors could be the potential reasons that lead to the poor correlations between the PSPA-USW and hydrodemolition data:

- The resolution of the PSPA contours (2x2 ft) is significantly lower than the LiDAR contours (0.02x0.02 ft). Increasing the resolution of PSPA contours with a denser test grid would likely improve the correlation but is not feasible from a practical perspective since the acquisition speed of PSPA system is relatively slow (30 seconds per point) from a bridge deck that is in service and where traffic control is required.

The absence of PSPA-USW data for the first 2 in. of the concrete bridge deck thickness (due to the limitations of sensor spacing as well as the range of analysis frequencies provided by PSPA: 0-50000 Hz) could be a potential reason leading to the

poor correlations since hydrodemolition removed less than 2 in. of concrete across most of the bridge deck (85%).

Results in Fig. 16 and the discussion above suggest that more work is needed to study the relationship between PSPA-USW and removal thickness data in order to be used for quantity estimations.

6. Conclusions

The hydrodemolition data presented in this paper provide comprehensive and relatively accurate information related to the deterioration conditions of the bridge deck, where weaker concrete was removed by high pressure water jets, and intact concrete was left in place. The in-situ elastic modulus of the concrete, which is directly related to the mechanical properties of the concrete (stiffness), was measured in the field by PSPA and for the first time compared with the hydrodemolition data. The effectiveness and limitation of the PSPA-USW method were assessed and summarized in this paper. More specifically:

- The average elastic modulus of the concrete bridge deck determined by the PSPA-USW method in deteriorated regions is significantly lower than in intact regions. The surface wave velocities (V_R) reduced significantly when they propagated into the defects of the concrete, which lead to lower average elastic modulus values for deteriorated concrete.
- The PSPA contours with 2x2 ft test grid were shown to be able to detect and characterize defects in the concrete bridge deck in this study; however, certainly the effectiveness of the PSPA contour is limited by the resolution. More information can be reveled with a dense test grid, however, this can be

challenging when data are to be acquired from a deck that is in service and traffic control is required.

- A qualitative correlation was identified and characterized between the USW and hydrodemolition test results. The areas of deteriorated concrete deck that were removed significantly during the hydrodemolition process were consistent with low average elastic modulus values characterized by the USW test.
- Analysis of the PSPA-USW elastic modulus and hydrodemolition data indicates that the PSPA-USW techniques could be a potentially effective method for estimating the thickness of concrete that would be removed during hydrodemolition. However, more work is needed to study the relationship between USW and removal thickness data in order to be used for quantity estimations.

Acknowledgments

This work was performed under the support of the Missouri Department of Transportation (MoDoT) and the National University Transportation Center (UNTC) at the Missouri University of Science and Technology (Missouri S & T). The authors would like to acknowledge Stanley Nwokebuihe, graduate student in Geological Engineering Department of Missouri University of Science and Technology, for his assistance in the data acquisition and processing. The authors would like to acknowledge Kenneth Boyko, graduate student in the Geological Engineering Department of Missouri University of Science and Technology, for his assistance in the LiDAR data acquisition and processing. The authors would also like to acknowledge Brandon Goodwin, graduate student in the Civil Engineering Department of Missouri University of Science and Technology, for his assistance in documenting of the concrete cores.

References

Azari, H., Yuan, D., Nazarian, S., and Gucunski, N., 2012. Sonic Methods to Detect Delamination in Concrete Bridge Decks. Transportation Research Record, No 2292, pp 113-124.

Azari, H., Nazarian, S., and Yuan, D., 2014. Assessing sensitivity of impact echo and ultrasonic surface waves methods for nondestructive evaluation of concrete structures. Construction and Building Materials, Vol. 71, pp 384-391.

Aggelis, D. G., and Shiotani, T., 2007. Repair evaluation of concrete cracks using surface and through-transmission wave measurements. Cement & Concrete Composites, No 29, pp 700-711.

Baker, M. R., Crain. K., Nazarian, S., 1995. Determination of pavement thickness with a new ultrasonic device. Research Report 1966-1, Center for Highway Materials Research, University of Texas, El Paso, pp. 69.

Gucunski, N., Slabaugh, G., Wang, Z., 2008. Impact echo data from bridge deck testing visualization and interpretation. Transportation Research Record, No. 2050, pp 111-121.

ICRI, 2004a. Guide for the preparation of concrete surfaces for repair using the hydrodemolition method. ICRI Technical Guideline No 310.3, International Concrete Repair Institute, Des Plaines, IL, 16 pp.

McDaniel, M., Celaya, M., Nazarian, S., 2010. Concrete Bridge Deck Quality Mapping with Seismic Methods-Case Study in Texas. Transportation Research Record, No. 2202, pp 53-60.

Malhotra, V. M., and Carino, N. J., 2004. Handbook on Non-destructive Testing of Concrete, second edition. CRC Press, New York, pp 386.

II. Condition Assessment of concrete pavements using both ground penetrating radar and stress-wave based techniques

Mengxing Li*
Department of Geological Engineering, Missouri University of Science and Technology, Rolla, MO 65409, Email: mlzg9@mst.edu

Neil Anderson
Department of Geological Engineering, Missouri University of Science and Technology, Rolla, MO 65409, Email: nanders@mst.edu

Lesley Sneed
Department of Civil, Architectural and Environmental Engineering, Missouri University of Science and Technology, Rolla, MO 65409, Email: sneedlh@mst.edu

Evgeniy Torgashov
Department of Geological Engineering, Missouri University of Science and Technology, Rolla, MO 65409, Email: evgeniy@mst.edu

ABSTRACT

Two stress-wave based techniques, ultrasonic surface wave (USW) and impact echo (IE), as well as ground penetrating radar (GPR) were used to assess the condition of a segment of concrete pavement that includes a layer of concrete, a granular base and their interface. Core specimens retrieved at multiple locations were used to confirm the accuracy and reliability of each non-destructive testing (NDT) result. Results from this study demonstrate that the GPR method is accurate for estimating the pavement thickness and locating separations (air voids) between the concrete and granular base layers. The USW method is a rapid way to estimate the in-situ elastic modulus (dynamic elastic modulus) of the concrete, however, the existence of air voids at the interface could potentially affect the accuracy and reliability of the USW test results. The estimation of the dynamic modulus and the P-wave velocity of concrete was improved when a shorter wavelength range (3 in. to 8.5 in.) corresponding to the concrete layer thickness was applied instead of the full wavelength rage (3 in. to 11 in.) based on the standard spacing of the receiver transducers. The IE method is proved to be fairly accurate in estimating

the thickness of concrete pavements. However, the flexural mode vibration could affect the accuracy and reliability of the test results. Furthermore, the existence of air voids between the concrete and granular base layers could affect the estimation of the compression wave velocity of concrete when the full wavelength range was applied (3 in. to 11 in.). Future work is needed in order to improve the accuracy and reliability of both USW and IE test results.

1. Introduction

The concrete pavement system in the United States is aging and deteriorating. Moisture with fine materials can easily enter the concrete pavement through the transverse and edge joints and corrode the reinforcement steel and erode the granular base material. In addition, severe exposure environments, such as freeze-thaw cycles and heavy traffic loading, can also deteriorate concrete and induce other serious problems. Accurate assessment of the condition of concrete pavement is critical for its maintenance. Non-destructive testing (NDT) methods have been widely used for this purpose since they are rapid, in-situ and non-destructive compared with traditional destructive testing methods.

In last two decades, numerous research and case studies were conducted with different NDT methods to monitor the conditions of concrete structures. Based on overall value, accuracy, ease of use and cost, ground penetrating radar (GPR), impact-echo (IE) and ultrasonic surface wave (USW) are three widely used and promising techniques (Gucunski *et al.,* 2013; Anderson *et al.,* 2015). Both USW and IE methods are based on generation of stress-waves and measurement of their velocities of propagation and other propagation characteristics such as reflection and dispersion. The USW method is used to

measure the phase velocity of Rayleigh waves and to estimate in-situ elastic modulus (dynamic modulus) of the material (Baker *et al.,* 1997; Nazarian *et al.,* 1997 and Celaya *et al.,* 2009). The IE method is used to locate defects as well as measure the thickness of the tested object (Cheng and Sansalone, 1999; Sansalone and Streett, 1997). On the other hand, the GPR method is based on generation of electromagnetic (EM) waves, measuring the velocity of EM waves and recording reflected EM waves in a tested object. The GPR method can be used to estimate pavement layer thickness and locate and estimate the depth of reinforcement steel (Al-Qadi and Lahouar, 2005). In other applications, the GPR method can be used to detect large size voids or delaminations in concrete pavement (Cassidy *et al.,* 2011; Liu *et al.,* 2008).

Many state transportation agencies still do not use NDT methods on a regular basis for monitoring concrete bridges or pavements conditions. Part of the reason is the complexity of data interpretation, especially when the existence of a potential defect is involved. In the case of stress-wave based methods (USW and IE), many factors can potentially affect the reliability of the data results, such as the size and depth of the defect, the flexural mode vibration, the geometry of the tested object and even the level of traffic noise in the field (Azari and Nazarian, 2015). Generally, analysis of IE data is focused on two types of vibration modes, the thickness mode (Lamb waves) and the flexural vibration mode. The flexural vibration mode tends to dominate the spectral response when an IE test is carried out over shallow defects, such as a delamination or air void in the pavement. This flexural vibration mode represents the out-of-plane vibration of the thin section of concrete above a delamination (Kee and Gucunski, 2016). On the other hand, for the GPR method, the moisture content, concrete condition, presence of highly

conductive material (clay) and size of the defect could affect the reliability of the test results (Maierhofer, 2003; Al-Qadi *et al.,* 2003).

Small air voids formed at the concrete-granular base interface are the most common type of defects characterized in jointed reinforced concrete pavement (JRCP), and they generally develop under transverse joints or pavement corners (Blaschke *et al.,* 1993). In recent years, several NDT methods have been used successfully by different researchers and transportation agencies to detect large-size void under rigid pavements, such as falling weight deflectometer (FWD) and impulse response methods (Nazarian *et al.,* 1994; Donahue, 2004). In order to evaluate the performance of different NDT methods to detect this type of defect and help state transportation agencies gain a better understanding of the relationship between NDT data and the condition of concrete pavement, in this paper, a combination of NDT (USW, IE and GPR) methods was used to monitor the condition of a jointed concrete pavement segment where the potential small separations (air voids) existence between the concrete and granular base layers. The visible evidence of the deterioration also appeared on the pavement surface (such as longitudinal and transverse cracks, transverse joint spalling). Core specimens retrieved at multiple locations were used to confirm the accuracy and reliability of each non-destructive testing (NDT) result. Furthermore, the variations and uncertainties of NDT data characterized in this study with potential causes are also summarized and presented.

2. The principle of the test methods

2.1. Ultrasonic surface wave (USW)

The USW method is used to estimate the Rayleigh wave phase velocity (V_R) in a given medium, such as a concrete slab (Baker *et al.,* 1995). The frequency range of

interest is limited to a high-frequency range where the Rayleigh wave's penetration depth is less than the thickness of the concrete slab. The USW method is based on impacting the surface of the concrete slab and recording the response of the slab with two receivers. Signal and spectral analyses are used to create the phase of cross power spectrum and the coherence function between the two receivers (Baker *et al.*, 1997). The variation of Rayleigh wave phase velocities with wavelength shorter than slab thickness is measured from the phase of cross power spectrum to generate a dispersion curve. Then the in-situ Young's modulus (dynamic elastic modulus) of the concrete slab can be calculated based on the following equation with an assumed or measured density and Poisson's ratio:

$$E = 2\rho[(1.13\text{-}0.16\nu)V_R]^2(1+\nu) \quad (1)$$

where:

V_R = phase velocity of Rayleigh wave

ρ = density

ν = Poisson's ratio

In the case of an intact concrete slab, the dispersion curve shows a relatively constant phase velocity with wavelength less than the slab thickness. In the case of a deteriorated concrete slab, the average phase velocity becomes less than that of an intact concrete slab, and the velocity obtained may be called an apparent velocity.

2.2. Impact echo (IE)

The impact echo method is commonly used to detect flaws in concrete as well as measure the slab thickness (Sansalone and Streett, 1997). The IE method is based on striking the concrete surface with an impactor, generating and transmitting stress waves at frequencies of up to 20 to 30 kHz and measuring the response by a nearby receiver.

The recorded time-domain signal is converted into a frequency-domain (amplitude spectrum) signal with the fast Fourier transform (FFT) analysis method. Then, the frequency of reflection, named "return frequency" is monitored. In the case of an intact concrete slab, the return frequency (*f*, also known as the thickness frequency) along with the measured or estimated compressional wave velocity V_p, can be used to estimate the slab thickness h with the following equation:

$$h = \beta\frac{V_P}{2f} \quad (2)$$

where:

$\beta = 0.96$ for concrete plates

V_P = compressional wave velocity

f = thickness frequency

h = slab thickness

The compressional wave velocity of concrete can be estimated based on the measured Rayleigh wave phase velocity with an assumed Poisson's ratio value:

$$V_P = (1.13\text{-}0.16\nu)V_R\sqrt{\frac{1-\nu}{0.5-\nu}} \quad (3)$$

where:

V_P = compressional wave velocity

V_R = Rayleigh wave phase velocity

ν = Poisson's ratio

Other reflectors could be voids, delaminations or various types of defects with different acoustic impedance than that of concrete. In the case of a deep delaminated area, the return frequency shifts to higher values than the thickness frequency. A wide or

shallow delaminated area is generally dominated by a peak frequency much less than the thickness frequency, indicating that a flexural-mode vibration dominates the frequency response. In this case, the slab thickness and the depth of the delamination cannot be calculated on the basis of Equation 2.

2.3. Ground penetrating radar (GPR)

The GPR method is used to record the reflected electromagnetic (EM) waves and estimate the propagation velocity of EM waves for a given medium (Maierhofer, 2003). When the EM energy propagates into the given medium, part of the energy is reflected and part is absorbed, depending on the dielectric contrast of the materials. The time delay and the amplitude of reflected signals can be used to evaluate the subsurface pavement conditions. Objects or areas in the subsurface with different electrical properties will reflect the waves differently and appear as anomalies. The EM velocity and the thickness of tested object can be calculated on the basis of the following equations:

$$V = \frac{c}{\sqrt{\varepsilon}} \quad (4)$$

$$h = \frac{V\Delta t}{2} \quad (5)$$

where:

V = velocity of EM waves

h = thickness of tested object

c = constant (speed of light in air = 0.30 m/ns)

Δt = time interval between peaks which represents the two-way travel time through the tested object

ε = dielectric constant of the material

The range of the dielectric constant for typical materials is summarized by Maierhofer (2003). It should be noted that the moisture content of the material can significantly affect its dielectric constant value. In general, the dielectric constant value of material with high moisture content is significantly higher than that of the same material in dry conditions.

3. Experimental site and test equipment

3.1. Experimental site and data collection

The experimental segment is located in the north bound lane of interstate highway I-55 in Missouri (Fig. 1). The segment is composed of a 9 in. thick jointed reinforced concrete pavement (JRCP) overlaid on a granular base material. The rebar mesh was placed in concrete layer at depth of 4 in. and the spacing between each transverse joint is 61.5 ft. Visible evidence of deterioration including longitudinal and transverse cracks, transverse joint spalling, patches and faulting was identified in the experimental segment, which is an indication the existences of potential defects in the concrete and granular base layers.

As illustrated in Fig. 2, both USW and IE data were acquired at 100 ft. intervals in the longitudinal (traffic) direction and 2 ft. intervals in the transverse direction of the experimental segment. A total of 62 USW and IE data points (including core locations) were acquired on the tested segment with a single operator in less than 2 hours. Additionally, GPR data were acquired at walking speed (3 mph) along 5 traverses oriented in the longitudinal direction with a 2 ft. spacing. Each GPR traverse was 1000 ft. long and overlapped with the USW and IE data points. GPR data were also acquired along certain transverse joints (perpendicular to traffic).

Fig. 1. Photo of the experimental segment.

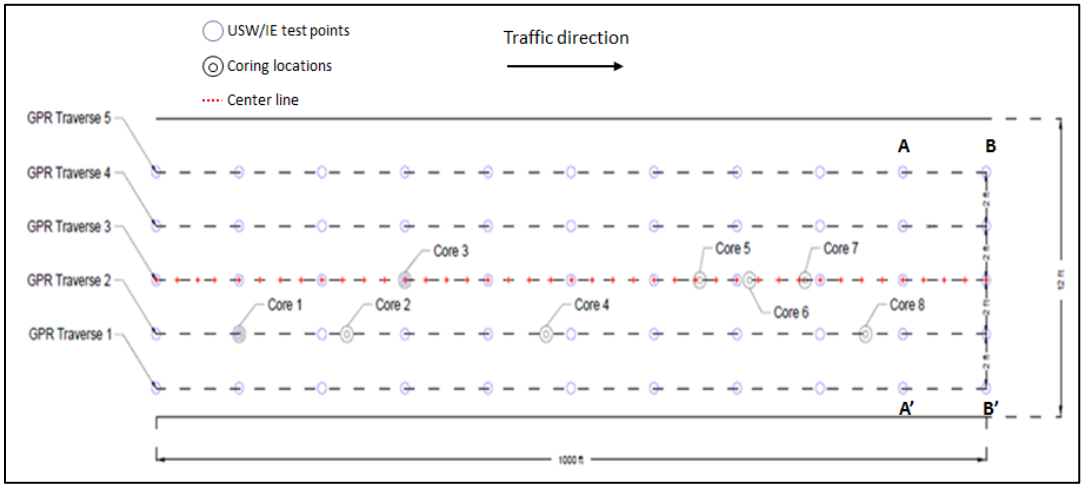

Fig. 2. Plan view map of the experimental site.

3.2. Test equipment

3.2.1. Portable seismic property analyzer (PSPA)

A commercially available ultrasonic acoustic device named a portable seismic property analyzer (PSPA) (Fig. 3a) was used for collecting both USW and IE data in the

field (Baker *et al.*, 1997). The PSPA consists of an impact source and two vertical receiver transducers packaged into a portable system that performs the USW and IE tests simultaneously on the basis of point loading. The device is connected to a laptop computer that controls the PSPA and automatically stores and interprets the acoustic signals recorded by the transducers. Each measurement took approximately taken 30 seconds in the field. The impact duration is approximately 130 μs and the data acquisition system has a sampling frequency of 390 kHz per channel.

The standard spacing of 6 in. between the two transducers was employed in this study, which provides a test wavelength range from 3 in. to 11 in. for building the dispersion curves of the USW test. The distance from the source to the near transducer is 4 in. An assumed value of density (150 pcf) and Poisson's ratio (0.18) for "good quality concrete" assigned by the PSPA-USW software was used to calculate the dynamic elastic modulus of top concrete in this study. The actual density of each concrete core specimen was measured in the laboratory. In general, the average actual density (147 pcf) of the core specimens was similar to the estimated density (150 pcf), which indicates that the estimated density of concrete used in the calculation of the dynamic modulus is fairly accurate. On the other hand, the effect of an assumed value of Poisson's ratio (0.18) on the accuracy of the calculated dynamic modulus is negligible since a wide variation of Poisson's ratio (0.1 to 0.25) will generate only ± 5% variation in dynamic modulus on the basis of Equation 1.

3.2.2. Ground penetrating radar (GPR)

A single cart-mounted high frequency (1.5 GHz) ground coupled antenna was employed for GPR data acquisition on the experimental segment (Fig. 3b). The GPR data

were acquired at slow walking speed (3 mph) in order to obtain high quality test results. The acquisition parameter employed was 512 samples/scan and 48 scans/foot. All of the GPR data were acquired in four hours. The raw GPR data were processed by the commercially available software RADAN 7.0 (RADAN 7 Manual, 2012) with an assumed dielectric constant for dry concrete (8.0) in order to convert reflection times to reflector depths.

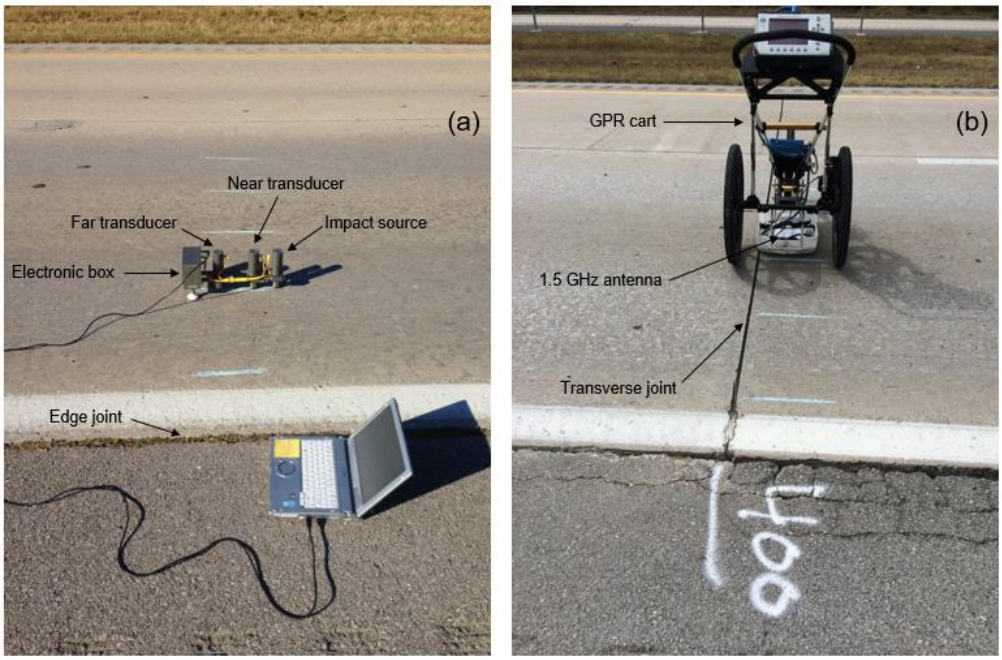

Fig. 3. Field test equipment employed in this study: a) PSPA b) Ground-coupled GPR.

4. Data presentation and analysis

4.1. USW data presentation and analysis

Typical waveform records and dispersion curves of the concrete pavement acquired at experimental site are illustrated in Fig. 4. In the case of station No. 05, the

Rayleigh wave phase velocities show constant with wavelengths (0.1 m to 0.28 m), and the interface between the concrete and granular base layers (0.23 m) cannot be identified from the dispersion curve. The waveform records of the far transducer have the same general shape as that of the near transducer, with a strong single-sine cycle at the front, which is representative of the first arrival time of Rayleigh waves. On the other hand, in the case of station No. 59, significant variations of Rayleigh wave phase velocities with wavelengths are identified in the dispersion curve. The phase velocities reduced significantly when the Rayleigh waves propagated into the granular base material (0.23 m – 0.28 m), which is an indication of potential separation (air void) or lack of contact between the concrete and granular base layers. The average phase velocity at station No. 59 (V_R = 2232 m/s) is lower than the average phase velocity (V_R = 2355 m/s) at station No. 05. The amplitude values of the waveform records of station No. 59 are half those of station No. 05, and the shape of the waveform is relatively wide. However, the first arrival time of Rayleigh waves can still be identified from the waveform records.

Core specimen #5 was retrieved at the same location as station No. 59, and photos of core #5 are illustrated in Fig. 5. In general, no visible evidence of a defect was identified in the concrete, however, small separations (air voids) between concrete and granular base layers were identified and measured (0.5 in. thick) in the field from the bottom of the borehole, which correlates well with the USW test results acquired at the same location.

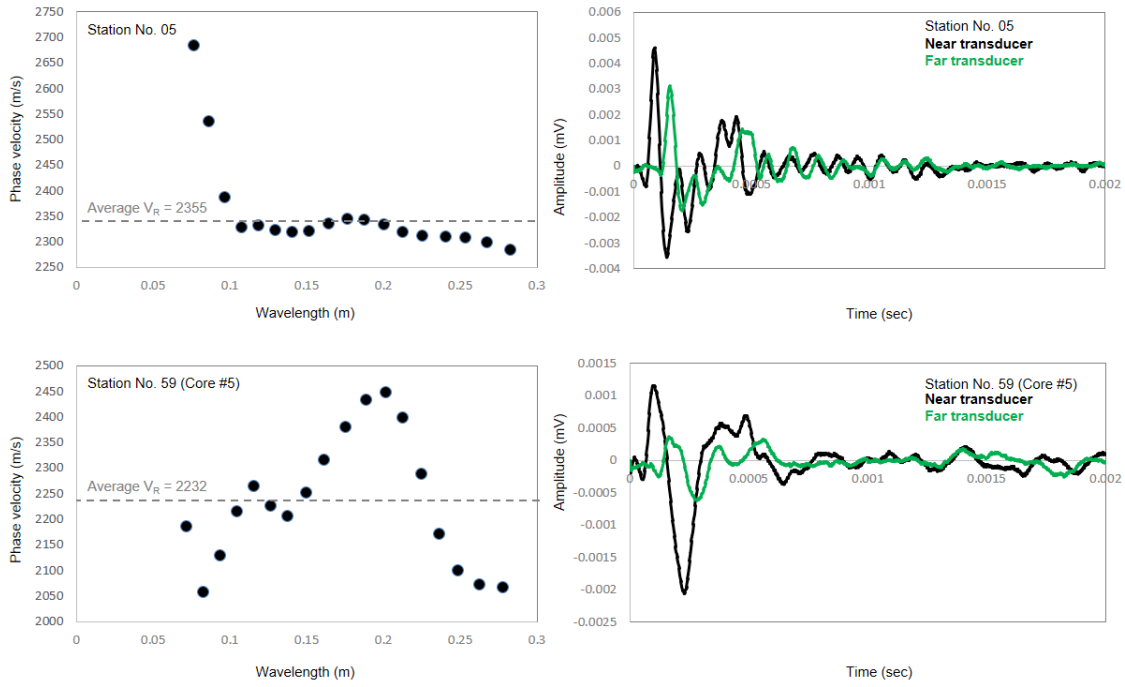

Fig. 4. Typical dispersion curves and waveforms records of USW tests acquired from the experimental segment.

Fig. 5. Photos of core #5 retrieved from the experimental segment.

Comparison of typical modulus curves (calculated based on dispersion curves) acquired at intact and deteriorated pavement locations are shown in Figure 6. It should be noted that the presented moduli distributions are calculated based on Equation 1 with assumptions of density and Poisson's ratio of the top concrete since the mechanical properties of concrete are relatively uniform, where precise distributions result from back-calculation of dispersion curves. At an intact pavement location (Figure 6, station No. 57), the moduli distributions are relatively constant with depth, and the concrete-granular base interface cannot be identified from the modulus curve. Considering the full wavelength range (3 in. to 11 in. based on the standard spacing of the receiver transducers), the average dynamic modulus E_{avg} is slightly higher than that at a deteriorated pavement location (Figure 6, station No. 61). At station No. 61, a significant dynamic modulus reduction (6820 ksi to 2026 ksi, 8 in. to 11 in.) was identified in the modulus curve when surface waves were propagated from the concrete to the granular base layers. Small separations (air voids) were identified in the bottom of the core #7 (0.5 in. thick), which correlates well with the dynamic modulus result. In this situation, the obtained dynamic modulus is underestimated and refers to an apparent modulus. On the other hand, it should be noted that the accuracy and reliability of the average dynamic modulus value could also be affected by the wavelength range. As shown in Fig. 6, for wavelengths shorter than 8.5 in., which corresponds to the concrete thickness, only slight differences could be identified between the two test points in term of average dynamic modulus and dispersion curves. In this case, the obtained average dynamic modulus E_{avg} of concrete is more consistent and reliable than the average dynamic modulus (E_{avg})

calculated based on full wavelength range since the influence of the under layer material (granular) and the deterioration (air voids) identified between their interface are excluded.

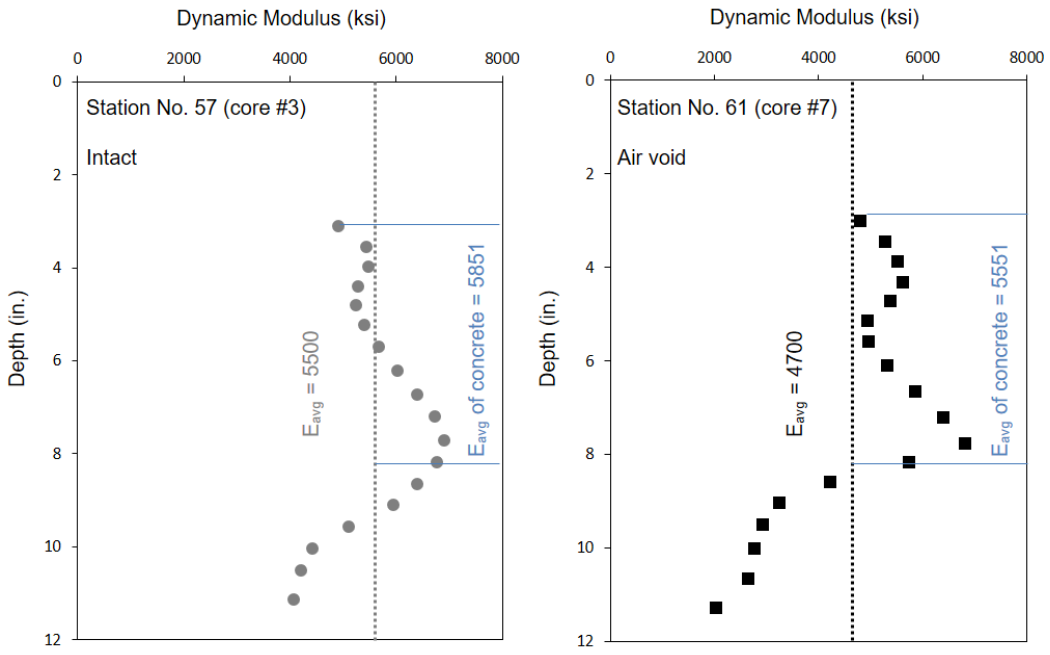

Fig. 6. Comparison of typical modulus curves acquired at intact and deteriorated pavement locations.

Since USW data were acquired at discrete points, it is often more effective to present the results in 2D contour images rather than to evaluate them individually. A 2D contour image can provide information about variations of pavement condition laterally as well as with depth. Representative 2D contour images of USW data acquired at section AA' and BB' (reference Fig. 2) are illustrated in Fig. 7. The dynamic modulus difference between the concrete and granular base layers cannot be distinguished in section BB', which is an indication of good contact between the concrete and granular base layers. On

the other hand, relatively low dynamic modulus values were identified at the base of the concrete layer in section AA', which is an indication of potential separation (air voids) between concrete and granular base layers.

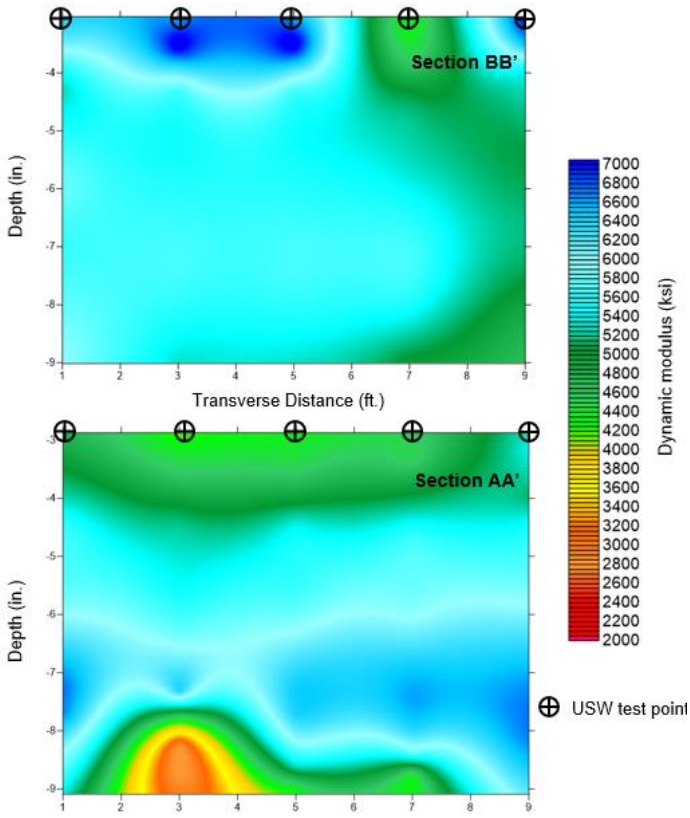

Fig. 7. 2D contour images of USW test results acquired at section AA' and BB' (Reference Fig. 2).

The average dynamic modulus values of the USW test points acquired in this study is fairly consistent (± 15%) according to the test results illustrated in Fig. 8. In general, values of the average dynamic modulus acquired at intact locations are slightly higher than those at deteriorated locations (air voids). However, for those USW test

points acquired at deteriorated locations (air voids), the estimated dynamic modulus was reduced significantly when the surface wave was approaching the interface between the concrete and granular base layers (Figure 7, section AA'), which is an indication of the potential deterioration (air voids) at the interface of concrete-granular base. In this case, the obtained dynamic modulus is underestimated and refers to an apparent velocity.

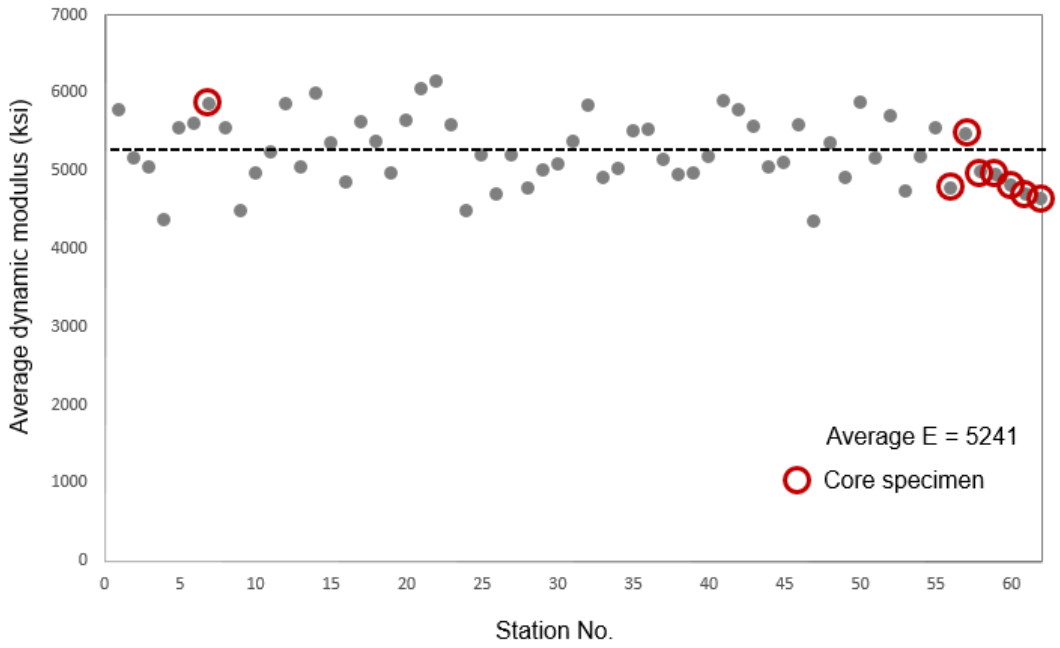

Fig. 8. Average dynamic modulus of the USW test points acquired from the experimental segment.

4.2. IE data presentation and analysis

Typical amplitude spectra of IE data acquired from the experimental segment are illustrated in Fig. 9. In the case of station No. 25, the amplitude spectrum was dominated

by the thickness frequency (9600 Hz), which is representative of the reflections from the bottom of the concrete layer. In the case of station No. 59, the thickness frequency (9800 Hz) was identified from the amplitude spectrum, which is representative of the reflections from the bottom of the concrete layer. In addition, a low frequency peak (800 Hz) was also identified from the amplitude spectrum. Core #5 was retrieved at the same location as station No. 59 (Fig. 5). No shallow delamination was identified in the concrete, but a small separation (air void) between the concrete and granular base layers was identified and measured from the bottom of the borehole (0.5 in. thick), which could be the cause of the low frequency peak identified in the amplitude spectrum. In the case of station No. 44, several low frequency peaks were identified in the amplitude spectrum, which is an indication the presence of a potential shallow delamination in concrete layer. In addition, the thickness frequency peak (10700 Hz) was still able to be identified from the amplitude spectrum, which corresponds to the reflections from the bottom of the slab. In the case of station No. 13, the flexural mode vibration (1000 Hz) dominated the frequency response, which is an indication the presence of a potential shallow delamination in the concrete layer. In this case, the slab thickness and the depth of the delamination cannot be calculated on the basis of Equation 2. Unfortunately, no core specimens retrieved at nearby locations of station No. 44 and No. 13 can prove the IE test results.

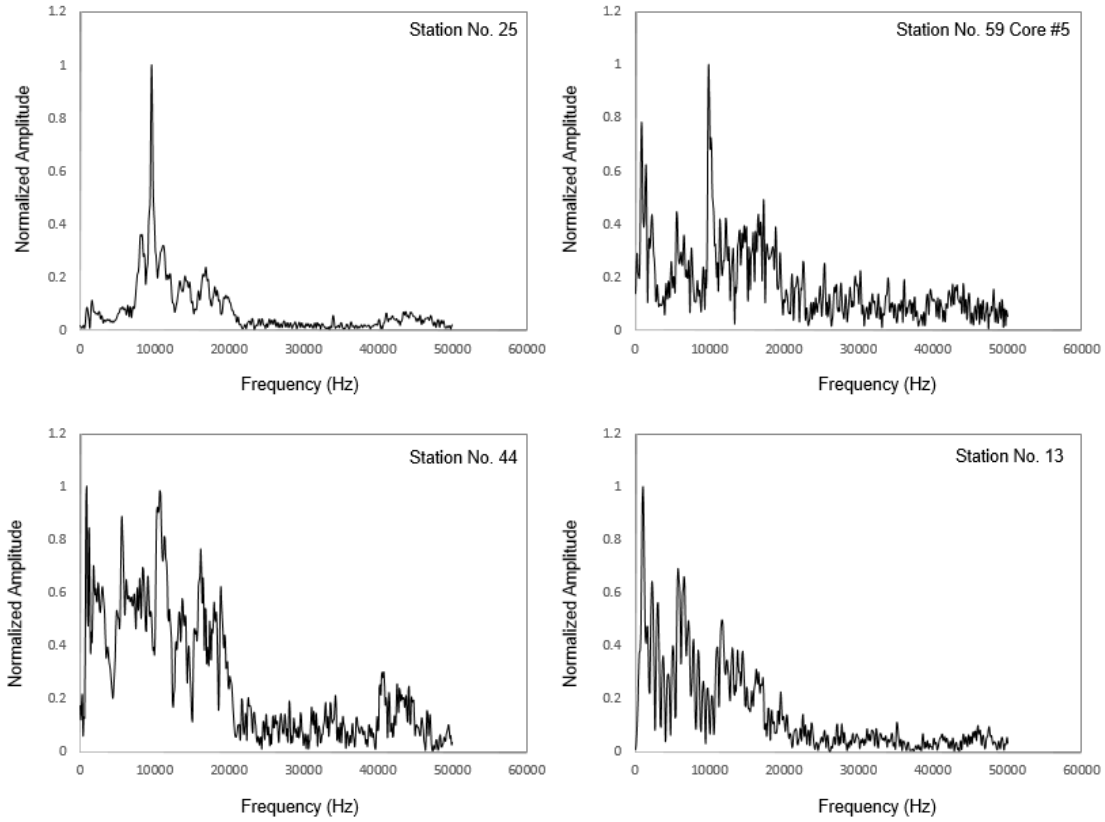

Fig. 9. Typical amplitude spectra of IE data acquired at experimental site.

The estimated pavement thickness calculated on the basis of Equations 2 and 3 is illustrated in Fig. 10. In general, the estimated thickness is fairly consistent (± 10%) when the scatter points due to the influence of flexural mode vibration are excluded. The estimated pavement thickness at core locations is 9.6 % lower, on average, than the actual pavement thickness. As shown in Fig. 11, the P-wave velocity of pavement at each location was estimated based on Equation 3 with an assumed Poisson's ratio value (0.18) of concrete. The accuracy of the estimated P-wave velocity could potentially be affected by several factors, including assumption of the Poisson' ratio value. More importantly, the estimation of the surface wave velocity (V_R) could be less accurate if the concrete or

the concrete-granular base interface is deteriorated. However, when the estimation of P-wave velocity is calculated based on shorter wavelength range (3 in. to 8.5 in.), which corresponds to the concrete thickness (8.5 in.), Fig. 11 shows that the estimated P-wave velocity values are relatively consistent and higher than the estimated P-wave velocity calculated based on the full wavelength range (3 in. to 11 in.).

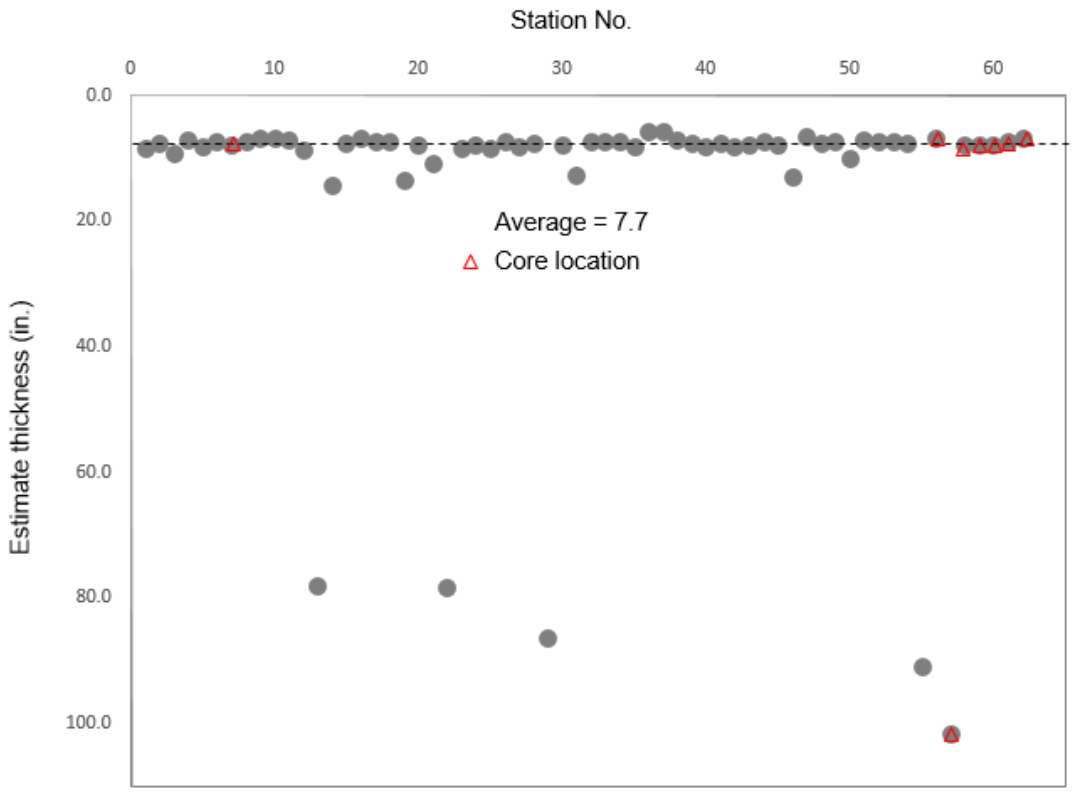

Fig. 10. The estimated thickness of the concrete pavements on the basis of IE data analysis.

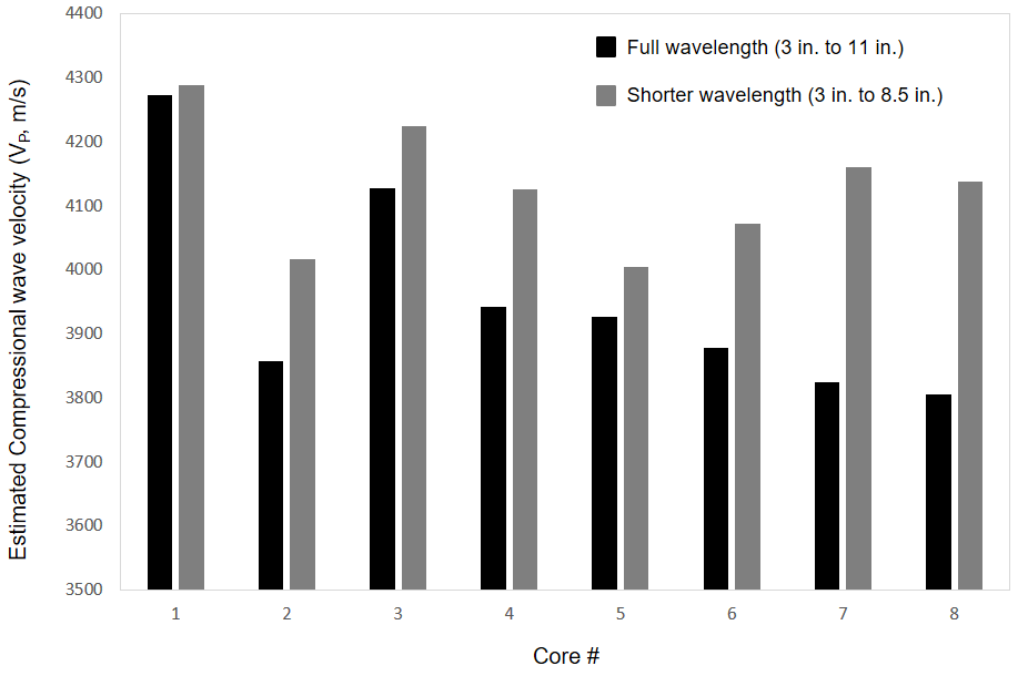

Fig. 11. The estimated P-wave velocity at each core location.

4.3. GPR data presentation and analysis

Typical GPR data acquired along the GPR transverse 2 are illustrated in Fig. 12. In the case of Fig. 12A, a reversed polarity of GPR signals was identified at the interface between the concrete and granular base layers, which is an indication of the potential separation (air void) between the concrete and granular base layers since the velocity of EM waves will increase when they propagate into the air void. On the other hand, the reversed polarity of GPR signals was not identified at the base of the concrete layer in Fig. 12B, which is an indication of the good contact condition between the concrete and granular base layers. Furthermore, the average dynamic modulus obtained from the

PSPA-USW tests at station No. 47 is significant lower than that at station No. 32, which could be the cause of the air voids identified in GPR profile.

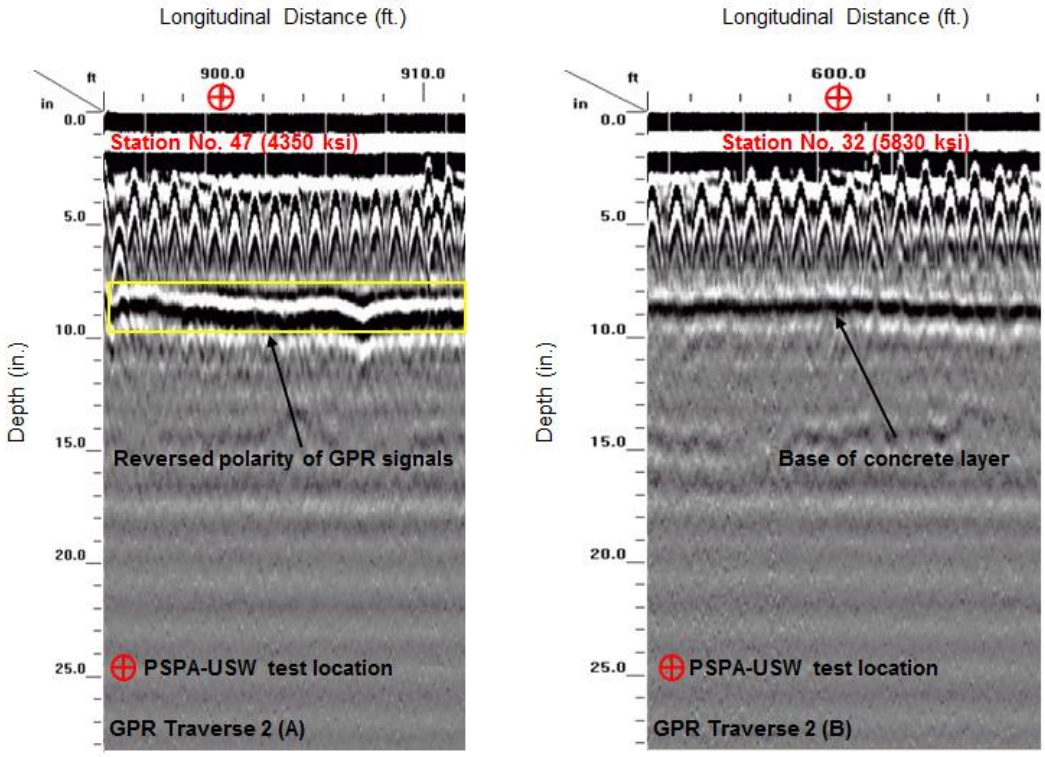

Fig. 12. Typical GPR data acquired at experimental site: A) deteriorated B) intact.

A comparison between the GPR section and core conditions retrieved at nearby locations is illustrated in Fig. 13. The reversed polarity of GPR signals was identified at the base of the concrete layer, which is an indication the presence of potential separations (air void) between concrete and granular base layers. On the other hand, no evidence of the deterioration was identified in the concrete based on core result, however, small

separations (air voids) between the concrete and granular base layers were identified and measured (0.5 in. thick) from the bottom of core location, which correlates well with the GPR test result.

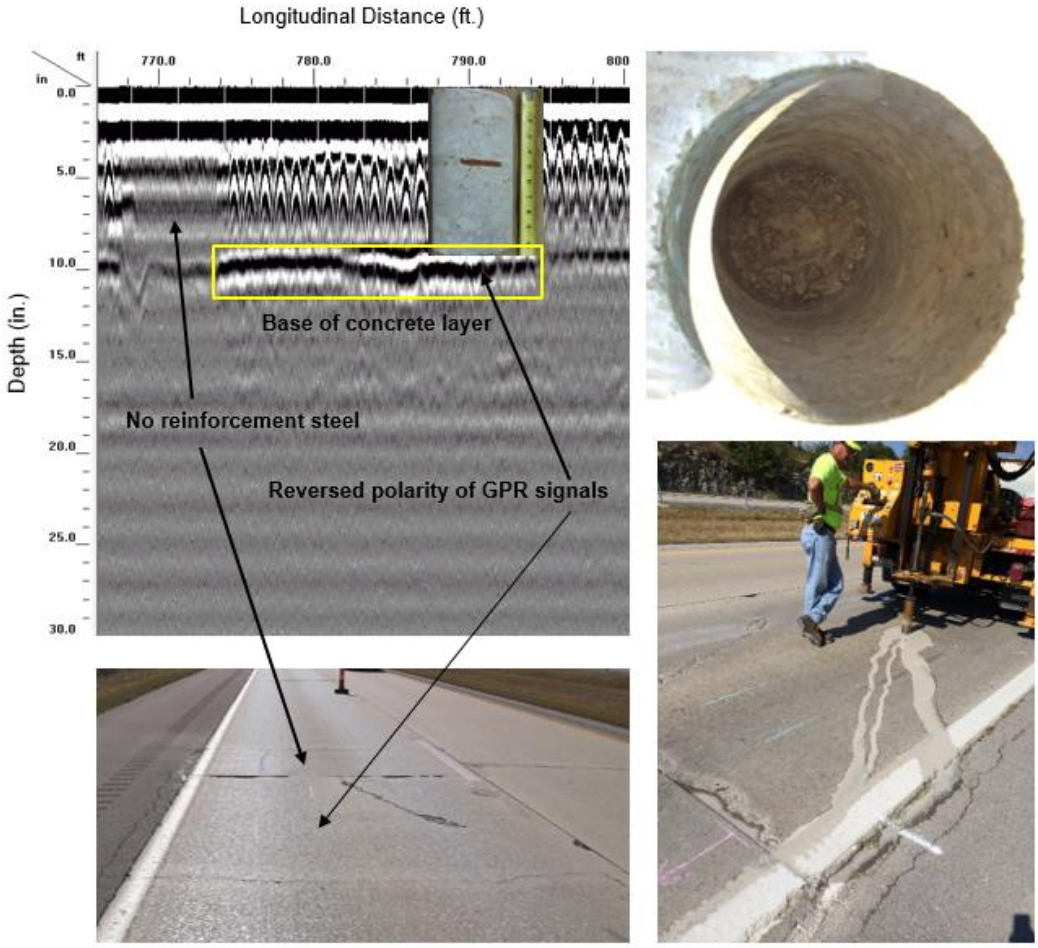

Fig. 13. Typical GPR data acquired at core locations.

A comparison between the estimated and actual pavement thickness based on the different NDT methods and core results is illustrated in Fig. 14. The estimated pavement

thickness of core #3 based on the IE data analysis was not available due to the influence of flexural mode vibration. In general, the estimated pavement thickness based on GPR method is more accurate and reliable than IE method in this case study.

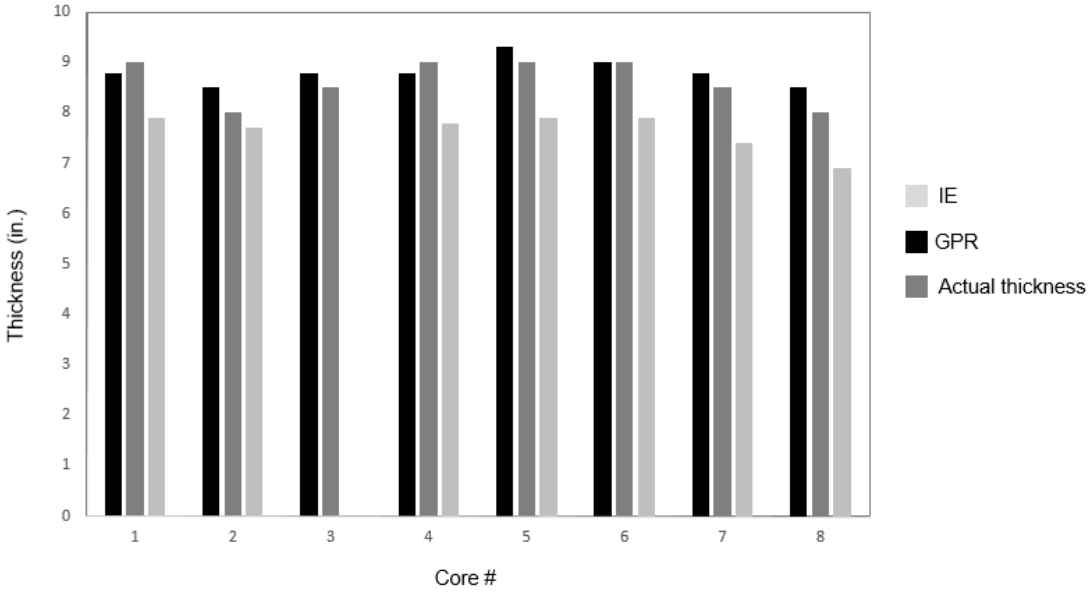

Fig. 14. Comparison of the pavement thickness estimation on the basis of NDT and core results.

The 2D contour image of pavement thickness estimated on the basis of GPR data acquired from the experimental segment is illustrated in Fig. 15. Areas with reversed polarity of GPR signals and absence of reinforcement steel are also highlighted in the figure. In general, most areas with reversed polarity of GPR signals were located beneath or along the transverse joint, which is an indication of the separations (air voids) between concrete granular base layers. Small separations (air voids) between the concrete and granular base layers were identified and measured (thickness varied from 0.25 to 0.5 in.)

at several core locations (core #4, #5, #6, #7 and #8), which correlates well with GPR test results. Furthermore, the dynamic modulus acquired at section AA' (900 ft. mark) is significantly lower than that at section BB' (1000 ft. mark), especially in the bottom of the concrete layer (Figure 7), which is induced by the air void based on GPR test result. In this situation, the estimated dynamic modulus is less accurate and refers to an apparent modulus.

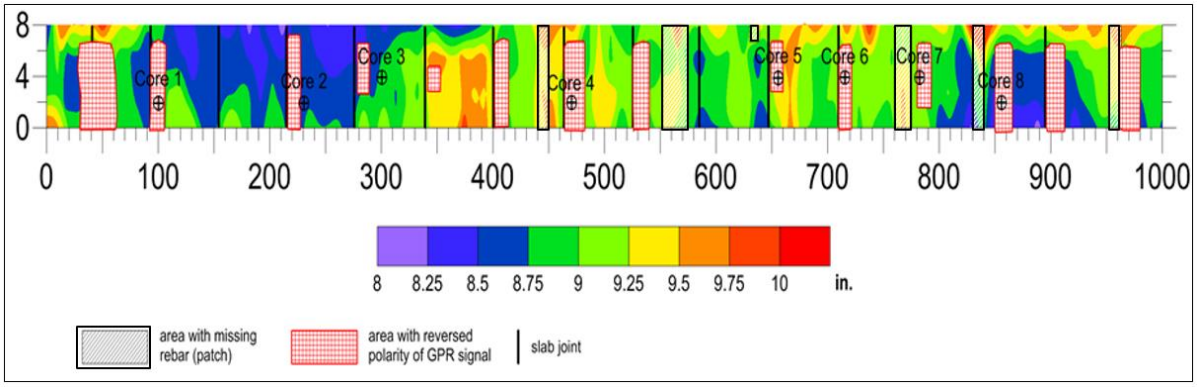

Fig. 15. The 2D contour images of the estimated pavement thickness on the basis of GPR data acquired from the experimental segment.

5. Conclusions

GPR is proved to be an accurate method used to estimate the thickness of concrete pavements in this study. Separations (air voids) at the concrete-granular base interface were successfully characterized by the reversed polarity of GPR signals and confirmed by core specimens retrieved at nearby locations. PSPA-USW is a rapid way to estimate the in-situ elastic modulus (dynamic elastic modulus) of the pavement, however, the

existence of air voids between concrete and granular base layers can affect the accuracy of the estimated Rayleigh wave phase velocities and dynamic elastic modulus. In this situation, the estimated dynamic modulus is less accurate and refers to an apparent modulus. The influence of deterioration (air voids) and the under layer material (granular base) on the estimation of the dynamic modulus and P-wave velocity of concrete can be reduced when a shorter wavelength range (3 in. to 8.5 in.) corresponding to the concrete thickness is used instead of the full wavelength range (3 in. to 11 in.) corresponding to the standard spacing of the receiver transducers. PSPA-IE is proved to be a fairly accurate method used to estimate the thickness of concrete pavements. However, the flexural mode vibration can affect the accuracy and reliability of the IE measurements. Furthermore, the existence of air voids between the concrete and granular base layers could affect the estimation of the compression wave velocity of concrete when the full wavelength range is applied (3 in. to 11 in.). More work and further studies are needed in order to improve the reliability and accuracy of both USW and IE test results.

Acknowledgements

The authors gratefully acknowledge the financial support of the Missouri Department of Transportation (TRyy1141), U.S. Department of Transportation (DTRT06-G-0014) and the National University Transportation Center (00039112) at the Missouri University of Science and Technology (Missouri S&T). The authors would also like to acknowledge Dr. Aleksey Khamzin, Dr. Aleksandra Varnavina and Stanley Nwokebuihe from the Geological Engineering Department of Missouri S&T, for their assistance with the GPR data acquisition and processing. Acknowledgements also go to Brandon Goodwin from the Department of Civil, Architectural and Environmental Engineering at Missouri S&T for his assistance with the visual inspection and documentation.

References

Al-Qadi, I., Lahouar, S., and Loulizi, A., 2003. Successful aplication of ground-penetrating radar for quality assurance-quality control of new pavements. Transportation Research Record, Vol. 1861, pp 86-97.

Al-Qadi, I., and Lahouar, S., 2005. Measuring rebar cover depth in rigid pavements with ground-penetrating radar. Transportation Research Record, Vol. 2005, pp 81-85.

Anderson, N., Sneed, L.H., Rosenblad, B., and Luna, R., 2015. MoDOT pavement preservation research program. Volume V, site specific pavement condition assessment. Report CMR16-004 v5, Missouri Department of Transportation, Jefferson City, MO, 641 pp.

Azari, H., and Nazarian, S., 2015. Optimization of acoustic methods for condition assessment of concrete structures. ACI Materials Journal, Vol. 112, No. 4, pp 569-577.

Baker, M., Crain, K., and Nazarian, S., 1995. Determination of pavement thickness with a new ultrasonic device: report for Texas Department of Transportation. Center for Highway Materials Research, University of Texas at El Paso, TX, 72 pp.

Baker, M., Nazarian, S., and Crain, K., 1997. Assessing quality of concrete with wave propagation techniques. ACI Material Journal, Vol. 94, pp 296-305.

Blaschke, B.C., Afferton, K.C., and Willett, T., 1993. AASHTO guide for design of pavement structures. American Association of State Highway and Transportation officials, Washington, D.C., 642 pp.

Cassidy N. J., Eddies, R., and Dods, S., 2011. Void detection beneath reinforced concrete sections: The practical application of ground-penetraing radar and ultrasonic technqiues. Journal of Applied Geophysics, Vol. 74, pp 263-276.

Chen, D.H., and Wimsatt, A., 2010. Inspection and condition assessment using ground penetraing radar. J. Geotech. Geoenviron. Eng., Vol. 136, pp 207-214.

Celaya, M., Nazarian, S., and Yuan, D., 2009. Comparison of field and laboratory strengths of concrete slabs. Non-Destructive Testing in Civil Engineering Conference, Nantes, France.

Cheng C.C., and Sansalone M., 1993. The impact-echo response of concrete plates containing delaminations: numerical, experimental and field studies. J Mater Struct, Vol 26, pp 274-285.

Donahue, J.P., 2004. Void detection with the falling weight deflectometer. Report RDT 04-004. Missouri Department of Transportation, Jeffrson City, MO, 34 pp.

Gucunski, N., Imani, A., Romero, F., Nazarian, S., Yuan, D., and Wiggenhauser, H., 2013. Nondestructive testing to identify concrete bridge deck deterioration. Report S2-R06A-RR-1. The second strategic highway research program, Washington, D.C. Transportation Research Board of the National Academies.

Kee, S.H., and Gucunski, N., 2016. Interpretation of flexural vibration modes from impact-echo testing. J. Infrastruct. Syst, 04016009, pp 1-10.

Liu, J.Y., Zollinger, D.G., and Lytton, R., 2008. Detection of delamination in concrete pavements using ground-coupled ground-penetrating rader technique. Transportation Research Record,Vol. 2087, pp 68-77.

Maierhofer, C., 2003. Nondestructive evaluation of concrete infrastructure with ground penetrating radar. Journal of Materials in Civil Engineering, Vol. 15, pp 287-297.

Nazarian, S., Yuan, D., Weissinger, E., and McDaniel, M., 1997. Comprehensive quality control of portland cement concrete with seismic methods. Transportation Research Record, Vol. 1575, pp 102-111.

Nazarian, S., Reddy, S., and Baker, M., 1994. Determination of voids under pavements using impulse response method. Nondestructive Testing, Vol. 2, pp 473-487.

RADAN 7 Manual, 2012. Geophysical Survey Systems, Inc., Salem, New Hampshire. http://www.uvm.edu/~lewebb/CCLI/Manuals/Radan7UserManual.pdf

Sansalone, M.J., and Streett W.B., 1997. Impact-echo: nondestructive evaluation of concrete and masonry. Ithaca, New York: Bullbrier Press.

III. An Assessment of Concrete Over Asphalt Pavement Using Both the Surface Wave and Impact Echo Techniques

Mengxing Li [1], Neil L. Anderson [2], Lesley H. Sneed [3] and Xin Kang [4, *]

[1] Department of Geological Engineering, Missouri University of Science and Technology, Rolla, MO 65409
Email: mlzg9@mst.edu

[2] Department of Geological Engineering, Missouri University of Science and Technology, Rolla, MO 65409
Email: nanders@mst.edu

[3] Department of Civil, Architectural and Environmental Engineering, Missouri University of Science and Technology,
Rolla, MO 65409
Email: sneedlh@mst.edu

[4] Department of Civil, Architectural and Environmental Engineering, Missouri University of Science and Technology,
Rolla, MO 65409
Email: xkb4c@mst.edu

*Now at TerraSense Geotechnical Lab LLC
Totowa, NJ 07512

ABSTRACT

A portable seismic property analyzer (PSPA) was used to simultaneously acquire both ultrasonic surface wave (PSPA-USW) and impact-echo (PSPA-IE) data at predetermined locations along a section of multi-layered pavement consisting of a basal concrete layer (~220 mm), an intervening layer of hot-mix asphalt (~60 mm) and a concrete overlay (~220 mm). The section of multi-layered pavement was cored at multiple PSPA test locations for verification purposes. The conditions of the extracted cores were assessed visually, and the static elastic modulus as well as the compressional wave velocity of each concrete overlay core were measured in the laboratory. Results from this study demonstrate that the PSPA-USW tool can be used to evaluate the

conditions of concrete overlay, the interlayer (hot-mix asphalt) as well as their bonding conditions from a qualitative perspective. A good correlation between the static and laboratory dynamic modulus of core specimens of concrete overlay were confirmed based on laboratory testing results. However, the field dynamic modulus of core specimens based on PSPA-USW tests was lower than both the static modulus and laboratory dynamic modulus. The PSPA-IE tool was not able to estimate the depth of the entire pavement and to various pavement layer interfaces due to the interference of flexural mode vibration. However, the difference between intact and deteriorated pavement can be qualitatively identified from the amplitude spectrum. More core specimens are needed for further studies in order to verify the performance of both PSPA-USW and PSPA-IE techniques for multi-layered pavement condition assessment.

Introduction

Stress-wave based non-destructive testing (NDT) methods have been used extensively for decades for estimating in-situ strengths (dynamic elastic modulus) of concrete structures (Hertlein, 2013). Ultrasonic pulse velocity (ASTM C597) and resonant frequency tests (ASTM C215) are two most popular NDT methods for this purpose. Numerous studies have been conducted in order to build the correlations of the results between the in-situ and traditional laboratory strength tests such as static elastic modulus test (ASTM C469) or compressive strength test (ASTM C39) for the same concrete. Generally, a strong correlation between the dynamic and static elastic modulus of concrete can be established, and the dynamic elastic modulus values are slightly higher than static elastic modulus values (Malhotra and Carino, 2004; Popovics et al., 2008). The difference in elastic modulus could be attributed to the inherent microstructure of concrete or the different ranges of measurements on the stress-strain curves.

Despite recent research progress, neither of the NDT methods mentioned above has been widely used by transportation agencies for estimating in-situ strengths of concrete bridges and pavements for several reasons: first, the acquisition speed for both NDT methods is relatively slow, and the strong background noise in the field (traffic, etc.) can affect the quality of test results. Second, a regular shape of concrete specimens (such as cylinders or blocks) is needed for both NDT tests in order to make good contact between the transducer and specimen surface. High quality test results can be obtained in laboratory since the level of background noise is significantly reduced compare to the field.

The portable seismic property analyzer (PSPA) is a rapid, non-destructive, in-situ testing device that simultaneously acquires both ultrasonic surface wave (PSPA-USW) data and impact echo (PSPA-IE) data in the field (Baker *et al.,* 1995). The ultrasonic surface wave method can be used to estimate the in-situ strength of concrete in an environment with strong background noise since the recognition of first arrival times of Rayleigh waves is much easier than compressional waves. The impact echo method can be used to estimate the pavement thickness as well as locate internal defects. The PSPA device is convenient to move in the field by one operator, and the data acquisition time for each test point is approximately 30 seconds.

In the last two decades, numerical studies demonstrated that the PSPA device can be successfully used to evaluate the conditions of concrete bridge decks and single layer concrete pavements in many cases (Baker *et al.,* 1997; Celaya *et al.,* 2007; Gucunski *et al.,* 2008; Hoda and Nazarian, 2015). However, the performance of the PSPA device used for the condition assessment of multi-layered concrete pavement has not been investigated. A comparison study (Celaya *et al.,* 2009) between the field (PSPA) and laboratory (ASTM C215) strengths for newly-constructed concrete slabs demonstrated that the field strengths were typically lower (average 15%) than laboratory strengths.

In an effort to determine whether the PSPA-USW test and the PSPA-IE test can be reliably used to assess the condition of multi-layered concrete pavement, the authors acquired PSPA data at multiple locations on a multi-layered concrete pavement along a two-lane highway. The laboratory static modulus test and ultrasonic test were conducted on core specimens of the concrete overlay in order to verify with PSPA-USW test results.

The actual thickness of each pavement layer was also measured and compared with the PSPA-IE test result.

Background Information

Portable Seismic Property Analyzer (PSPA)

The portable seismic property analyzer (PSPA), as illustrated in Fig. 1, is an integrated ultrasonic acoustic device designed to: 1) measure vertical variations in the dynamic elastic modulus (Young's modulus) of a given medium; 2) estimate the thickness of the medium; and 3) detect and locate flaws within the medium (Baker *et al.,* 1995).

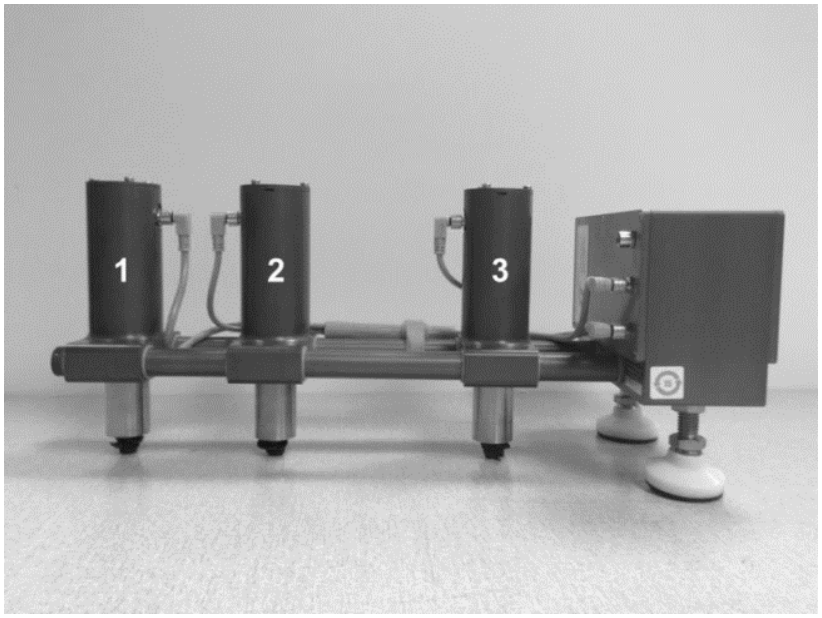

Figure 1. Portable seismic property analyzer (PSPA): 1) impact source; 2) near transducer; and 3) far transducer.

The PSPA consists of an impact source and two vertical transducers packaged into a portable system that performs USW and IE tests simultaneously. The device is connected to a laptop computer that controls the PSPA and automatically stores and interprets the acoustic signals recorded by the transducers (Baker *et al.*, 1997). The sampling frequency of PSPA system is 390 kHz/channel, and the impact duration is approximately 130 μs.

Ultrasonic Surface Wave (USW)

The PSPA-USW test measures the phase velocities of Rayleigh waves propagating through the medium to a maximum depth that is a function of the spacing between the receiver transducers (Baker *et al.*, 1997). The PSPA-USW test is based on striking the surface of the tested object and recording the response of the object with two transducers. The variation in Rayleigh wave phase velocity (V_R) with wavelength shorter than the thickness of tested object is measured to generate a dispersion curve. V_R is determined by dividing the distance between two transducers (Δx) by the difference in the arrival time of a specific wave (Δt). Then the average elastic modulus for a uniform material can be calculated based on the following equation with assumed values of density and Poisson's ratio:

$$E = 2\rho[(1.13-0.16\nu)V_R]^2(1+\nu) \quad (1)$$

where:

V_R = phase velocity of Rayleigh wave

ρ = density

ν = Poisson's ratio

For each PSPA test, the solenoid-type source with two transducers needs to be coupled on the concrete surface by the operator in the field in order to obtain high quality test results. In case of an intact concrete slab, the dispersion curve shows relatively constant Rayleigh wave phase velocity within the wavelengths less than the slab thickness. When the concrete is deteriorated, the average Rayleigh wave phase velocity becomes less than that of intact concrete due to the interference caused by the defects.

Impact-echo (IE)

The impact echo (IE) test is designed to detect flaws and estimate layer thicknesses in a given medium, such as concrete slabs (Sansalone and Streett, 1997). The test is based on striking the surface of the tested object with an impact source, generating and transmitting stress waves at frequencies of up to 20 to 30 kHz, and measuring the response by a nearby transducer. The PSPA-IE test is conducted using the impact source and near-offset transducer as shown in Fig. 1. The recorded time-domain signal is converted into a frequency-domain function using fast Fourier transform (FFT) analysis, and the frequency of reflection, named “return frequency”, is monitored. In the case of an intact concrete slab, the “return frequency” (f_r, also known as the resonance frequency) along with the estimated compressional wave velocity V_P can be used to estimate the thickness of concrete slab (T) with the following equation:

$$T = \alpha \frac{Vp}{2 \times fr} \quad (2)$$

where:

T = thickness

V_P = compressional wave velocity

f_r = resonance frequency

α = 0.96 (constant for plate-like structure; Gibson *et al.*, 2005)

The average Rayleigh wave phase velocity of the tested object based on PSPA-USW tests, along with the assumed value of Poisson's ratio can be used to estimate the compressional wave velocity with the following equation:

$$V_P = (1.13\text{-}0.16\nu)V_R\sqrt{\frac{1-\nu}{0.5-\nu}} \quad (3)$$

where

V_P = compressional wave velocity

V_R = average Rayleigh wave phase velocity

ν = Poisson's ratio

In the case of a deteriorated concrete slab, other reflectors could be a void, delamination, or various types of defects with different acoustic impedance than that of concrete. In the case of a concrete slab with a wide or shallow delamination, a flexural mode response will dominate the frequency response with a peak frequency less than the resonance frequency, indicating that little or no energy propagates toward the bottom of the concrete slab (Cheng and Sansalone, 1993). In this case, the thickness of concrete slab cannot be estimated according to the Equation 2.

Ultrasonic Velocity Testing System

Ultrasonic testing is non-destructive and provides compressional (P) wave and shear (S) wave velocity information that can be used in calculating dynamic elastic constants such as Poisson's Ratio (ν), Young's Modulus (E), Bulk Modulus (K), and Shear Modulus (G).

The Ultrasonic Velocity Test System (Fig. 2) was employed in this study to perform the ultrasonic velocity measurements on concrete overlay core specimens.

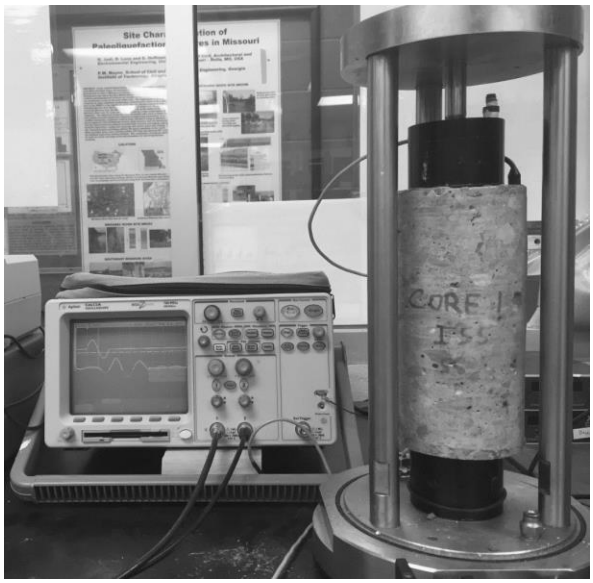

Figure 2. Ultrasonic velocity testing system.

The travel time (T) of P-wave is determined by using the starting time of the sinusoidal input wave and subtracting the first arrival time of the received signal. The length of the specimen (L) over the travel time yields the P-wave velocity, as shown in Equation 4. The Young's modulus of the specimen is determined by Equation 5.

$$V_P = \frac{L}{T} \quad (4)$$

$$E = \rho V p^2 \quad (5)$$

Where:

V_p = compressional wave velocity

L = length of the specimen

T = travel time of compressional wave

ρ = density

Static Elastic Modulus Testing

The standard test method for static modulus of elasticity of concrete (ASTM C469) was employed in this study for measuring the static elastic modulus of the concrete overlay core specimen (Fig. 3). This test method can be used to determine chord modulus of elasticity (Young's) and Poisson's ratio of diamond-drilled concrete cores when under longitudinal compressive stress. The calculation of the modulus of elasticity to the nearest 200 MPa is based on the following equation:

$$E = (S_2 - S_1) / (\varepsilon_2 - 0.000050) \quad (6)$$

where:

E = chord modulus of elasticity, MPa

S_2 = stress corresponding to 40% of ultimate load

S_1 = stress corresponding to a longitudinal strain, ε_1, of 50 millionths, MPa

ε_2= longitudinal strain produced by stress S_2

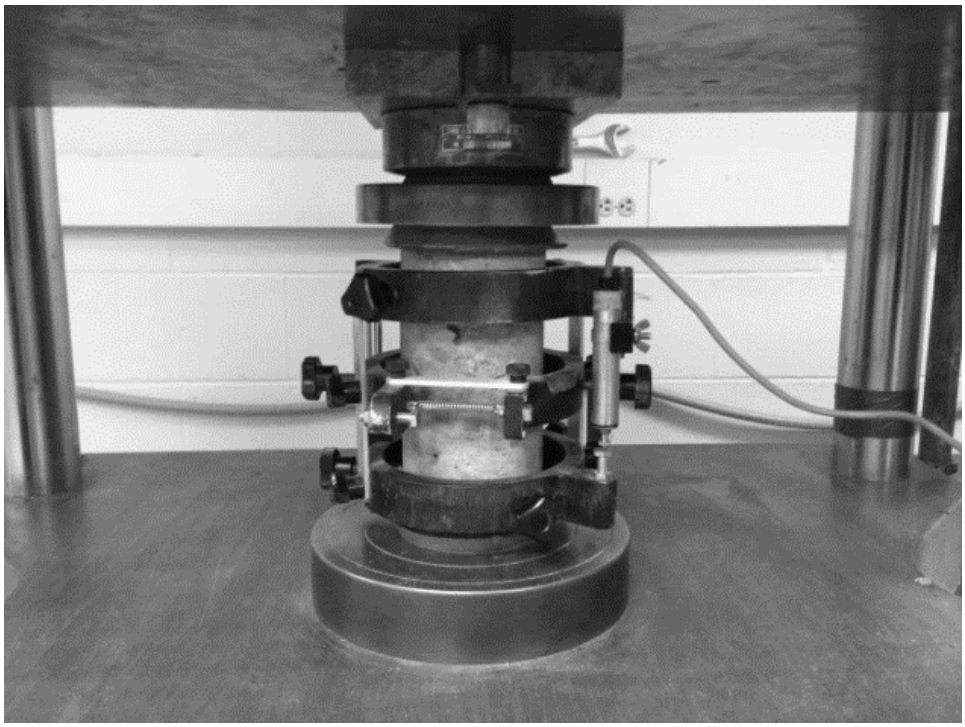

Figure 3. The static elastic modulus of concrete overlay of core specimens was determined by the standard test method procedure (ASTM C469).

Case Study Description and Data Collection Methods

Description of Test Site

The test site was a 305 m segment of a two-lane roadway located in southeast Missouri shown in Fig. 4. The tested pavement consists of a ~220 mm of portland cement concrete (PCC; herein referred to as concrete) overlay above a ~220 mm thick unbonded basal concrete layer. A ~60 mm thick layer of hot mix asphalt (HMA; herein referred to as asphalt) is embedded between the two concrete layers. The concrete overlay displayed no visible evidence of surface cracks. However, possible degradation was suspected in the intervening asphalt layer based on results of previous investigations.

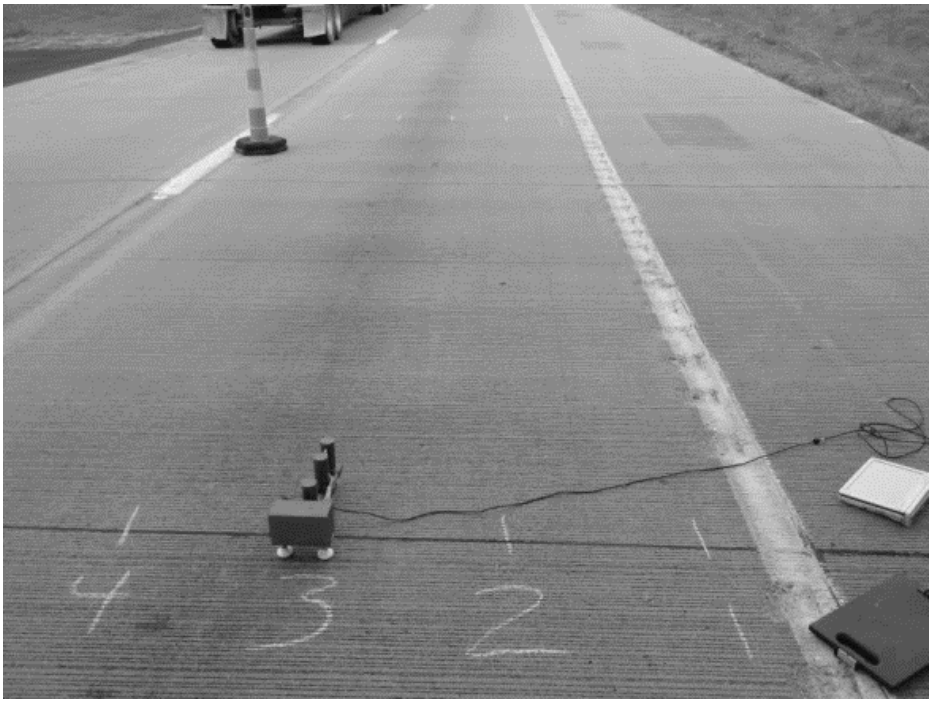

Figure 4. Photo of experimental site.

Data Acquisition

As shown in Fig. 5, PSPA data were acquired on the top surface of the pavement at 30.5 m intervals in the longitudinal direction (parallel to the traffic direction) and 0.6 m intervals in transverse direction (perpendicular to the traffic direction). Additional PSPA data were also acquired at the selected core locations. In total, PSPA data were acquired at 62 locations. The PSPA device was oriented parallel to the longitudinal direction of the roadway. The standard 150 mm spacing between the two transducers was used in order to obtain the maximum effective investigation depth (80 mm to ~280 mm). A single operator acquired all of the PSPA data in less than 2 hours.

Eight 100 mm diameter cores were extracted from the pavement. Core locations are shown in Fig. 5. The cores were photographed and documented in terms of layer type

and thickness, visible flaws, interfacial bond and stripping (asphalt layer). Interfacial bond was determined qualitatively by the force required to break the bond between the layers; degree of stripping was determined by careful examination of a longitudinal split-section of the asphalt layer of the core.

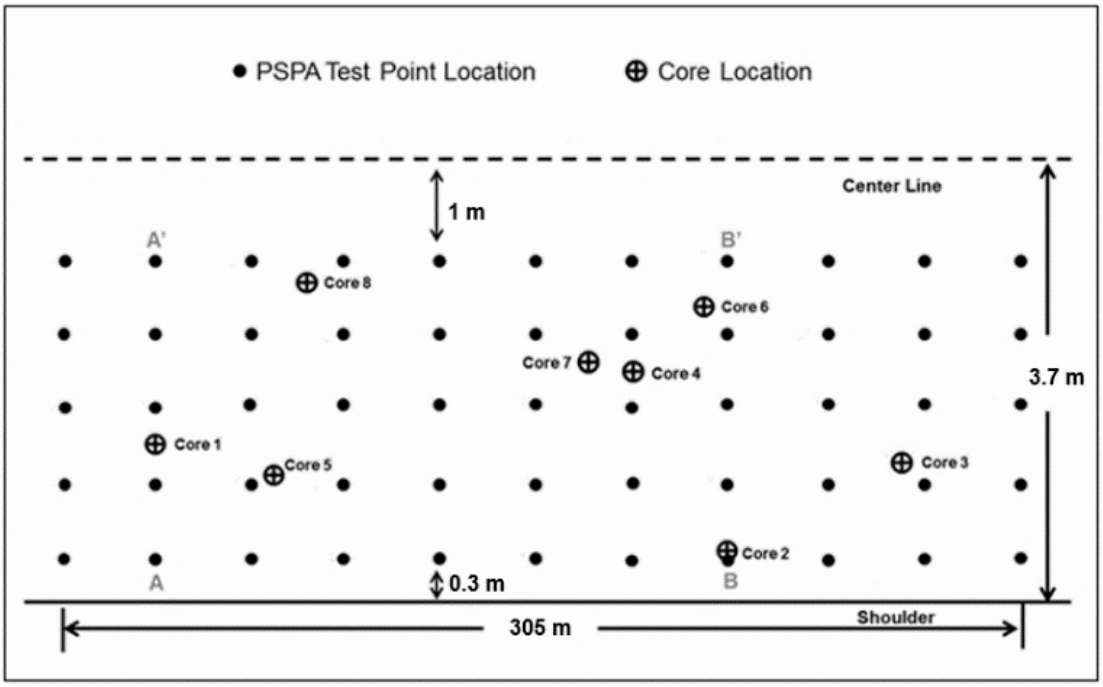

Figure 5. Schematic of PSPA test point locations at experimental site.

Data Presentation and Analysis

Summary of Core Evaluations

Photos of typical intact and deteriorated core specimens are illustrated in Fig. 6. No visible evidence of deterioration was identified in either concrete layers, with the exception of voids. For an intact core specimen (Fig. 6b), the interface between the

concrete overlay and asphalt layer was well-bonded, and no visible evidence of deterioration was identified in asphalt layer. For the deteriorated core specimen shown in Fig. 6a, the asphalt layer was stripped at the depth of 230 mm, which is near the interface between the concrete overlay and asphalt layer.

Figure 6. Photos of typical deteriorated (a) and intact (b) core specimens retrieved from experimental site.

The correlation between the average dynamic elastic modulus (based on 18 USW measurements) and condition of core specimens retrieved from the experiential site is summarized in Table 1. Break loading tests were conducted on core specimens in order to

determine the relative bond strength of the interface between the concrete overlay and intermediate asphalt layer as well as the strength of asphalt layer. In general, a good correlation between the average dynamic modulus and condition of core specimens can be established where higher modulus correlated well with strong bond conditions.

Table 1. Correlations between the average dynamic elastic modulus and deterioration conditions of core specimens.

Core #	E_{avg} (GPa)	Evaluation of bond at concrete overlay/asphalt interface	Evaluation of stripping in asphalt layer
1	26	NA	Moderate stripping
2	29	Debonded	None
3	34	Strong bond	None
4	27	Weak bond	None
5	30	Moderate bond	None
6	37	Strong bond	None
7	28	Moderate bond	None
8	37	Strong bond	None

PSPA-USW Test Results

Typical full waveform records and dispersion curves of intact (Core #6) and stripped (Core #1) core specimens are presented in Fig. 7 and 8. For an intact core specimen (Fig. 7, Core #6), the waveform record of the far transducer has the same general shape as that of the near transducer, with a strong single-sine cycle at the front, which is representative of the first time arrival of Rayleigh waves. For a stripped core

specimen (Fig. 7, Core #1), the amplitude of the waveform records of the far transducer is twice as large as that of Core #6 (far transducer). A second larger cycle in the waveform records of far transducer is recognized except the first cycle (Rayleigh wave), which is probably representative of the arrival of the flexural mode waves induced by stripping in the asphalt layer since the flexural mode waves generally travel more slowly than Rayleigh waves.

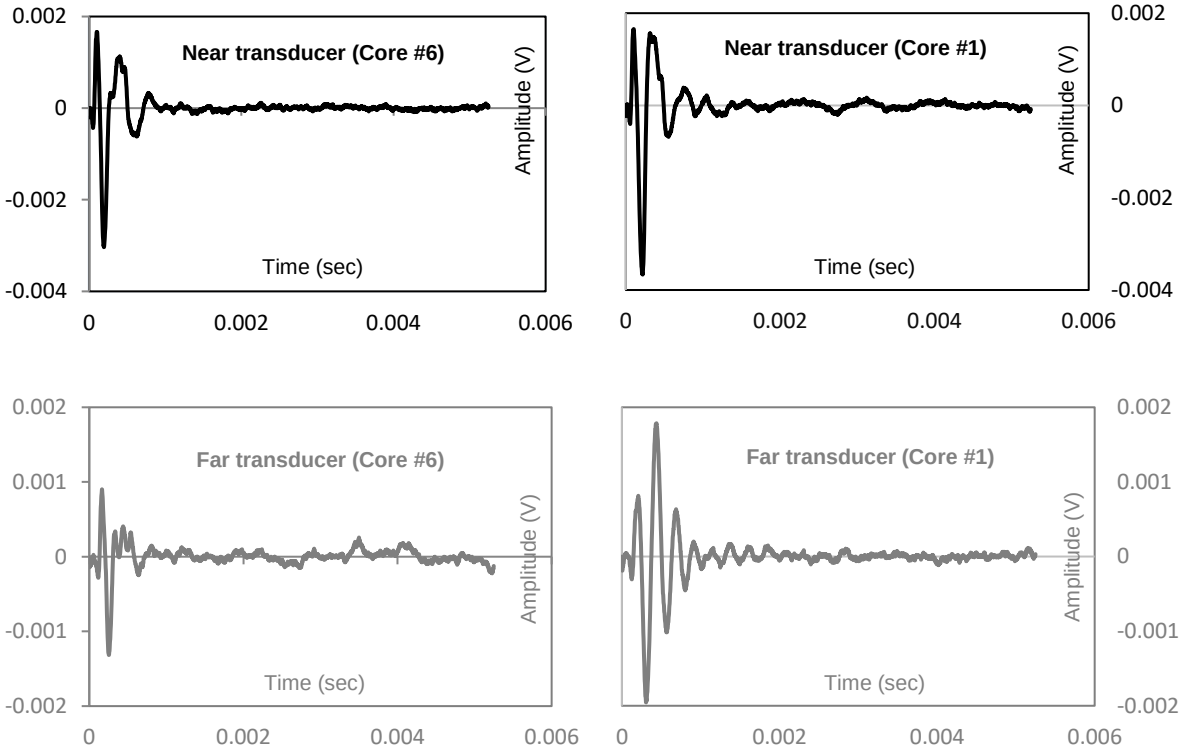

Figure 7. Typical full waveform records of intact (Core #6) and stripped (Core #1) core specimens.

The dispersion curve of Core #6 (Fig. 8) shows relatively constant phase velocities with wavelengths ranging from 0.08 m to 0.28 m. However, the interface between the concrete overlay and asphalt layers cannot be identified from the dispersion curve. The average phase velocity of Core #1 (1923 m/s) is much lower than that of Core #6 (2312 m/s). A Rayleigh wave phase velocity reduction at the depth of 0.2 m was identified in dispersion curve of Core #1, which is probably induced by flexural mode waves. The flexural mode wave induced by stripping (0.23 m) can distort PSPA-USW analysis and absorb PSPA-USW energy at the wavelength approaching the stripping location, which is caused the reduction of phase velocities in dispersion curve. In this situation, the measured phase velocity may refer to an "apparent velocity".

The dynamic elastic modulus of each PSPA test point was calculated based on Equation 1 with an assumed value of density (2400 kg/m^3) and Poisson's ratio (0.18) for concrete in this study. The effect of an assumed value of Poisson's ratio on the accuracy of the calculated dynamic modulus can be neglected since a wide variation of Poisson's ratio (0.1 to 0.25) will generate only ± 5% variation in dynamic modulus based on Equation 1. The actual density of each core specimen of concrete overlay was measured in laboratory, and their values were slightly lower than assumed density (1.7% to 4.6%), which is indicates that the assumed density of concrete is fairly accurate in the calculation of the dynamic elastic modulus.

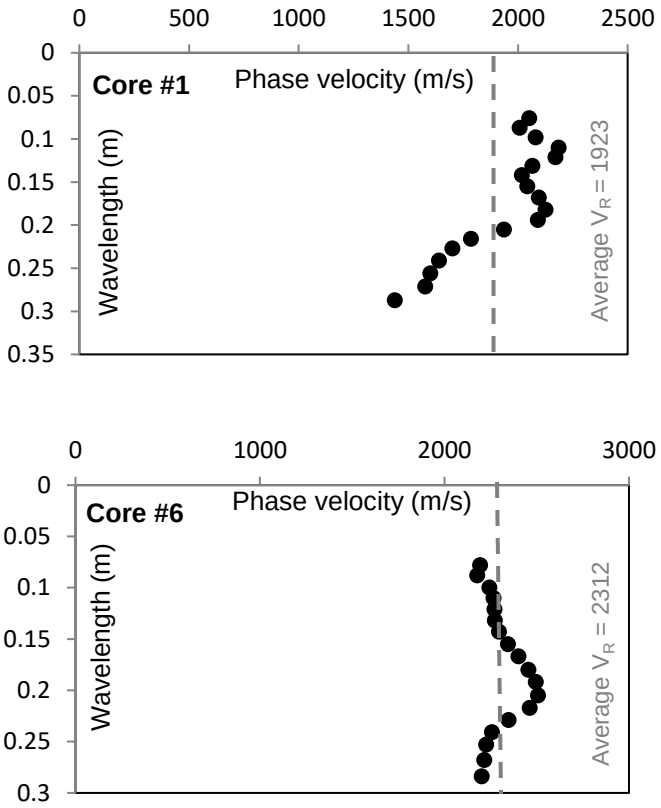

Figure 8. Typical dispersion curves of intact (Core #6) and stripped (Core #1) core specimens.

A large variation of dynamic modulus (± 18%) was identified in Fig. 9 with an average dynamic elastic modulus of 34 GPa for all PSPA test points acquired in this study. Several potential factors could contribute to the variation of dynamic modulus: first, the bond conditions (debonded or weak bonded) between the interface of concrete overlay and intermediate asphalt layer; second, it is possible that defects (such as delamination or stripping) exist in both concrete layers and the asphalt layers. Each of these possible conditions could induce the flexural mode waves and affect the accuracy of the PSPA-USW test results.

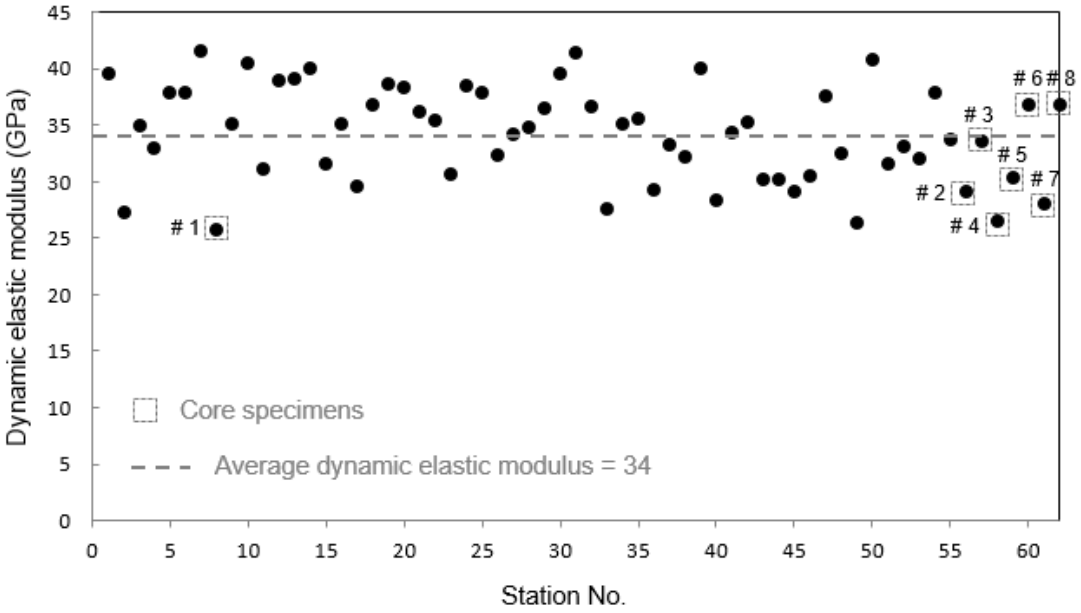

Figure 9. Average dynamic elastic modulus of all PSPA test points collected at experimental site.

Since PSPA-USW data were acquired at discrete points, it is often more effective to present the results in 2D contours rather than to evaluate them individually. A 2D contour can provide information about variations of pavement condition laterally as well as with depth. As shown in Fig. 10, representative 2D contours acquired at Section AA' and Section BB' (reference Fig. 5) demonstrated the variations of dynamic modulus with wavelength from 80 mm to 230 mm. Deteriorated concrete was identified by relatively low dynamic modulus and confirmed by core specimens, especially in the bottom of the concrete overlay (220 mm).

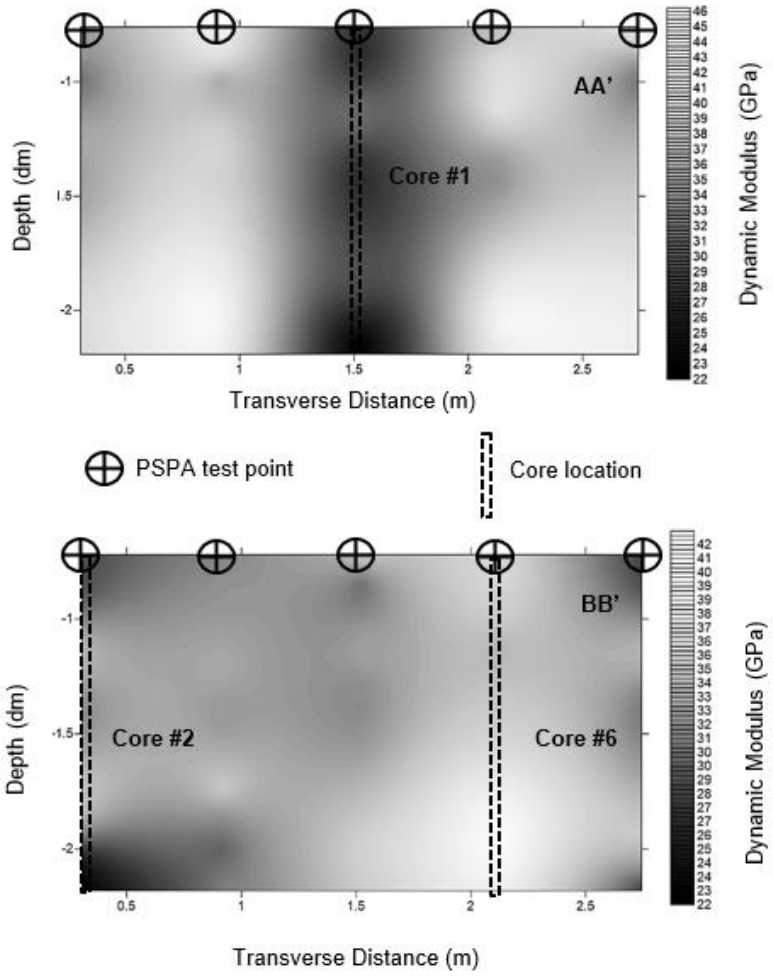

Figure 10. 2D contours of the dynamic elastic modulus (GPa) for the upper concrete layer acquired from Sections AA' and BB' (Fig. 5).

Static Elastic Modulus Testing

In order to evaluate the reliability of PSPA-USW test results (dynamic elastic modulus), the static elastic modulus of the concrete overlay core specimens was measured in laboratory based on the standard test procedure for static modulus of elasticity for concrete cylinders (ASTM C469). The static elastic modulus of asphalt core specimen cannot be measured due to the limitation of specimen length. Two concrete overlay core specimens (Core #4 and Core #8) were used to determine the compressive

strength in accordance with standard test method (ASTM C39) prior to the test for modulus of elasticity. As shown in Fig. 11, the compressive strength of Core #4 was obtained (49 MPa) with a peak load of 40620 kg. A typical stress-strain curve of a concrete overlay core specimen (Core #1) is illustrated in Fig. 12. The specimen was loaded three times, and only the records of last two loadings were used to calculate the modulus of elasticity based on Equation 6. Fig. 12 shows the loading and unloading branches of the three loadings. In general, the dynamic elastic modulus is slightly higher than the static modulus for the same concrete specimen since it represents a measurement at low strain level (10^{-6}); on the other hand, the ASTM measurements are typically not performed at this levels because of the mechanical limitations in the measurement of the strain.

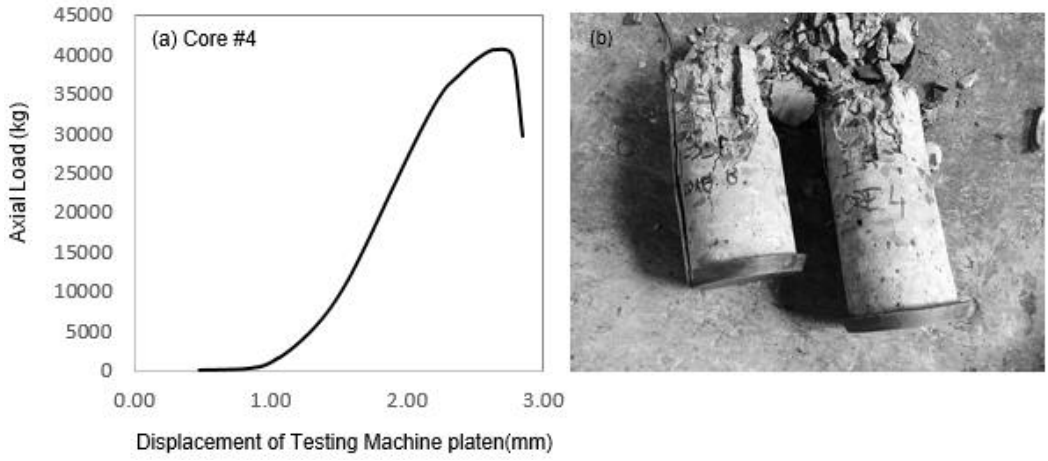

Figure 11. a) Typical axial loading curves of concrete overlay core specimen during the standard compressive strength test b) Photos of concrete overlay core specimens after compressive strength test.

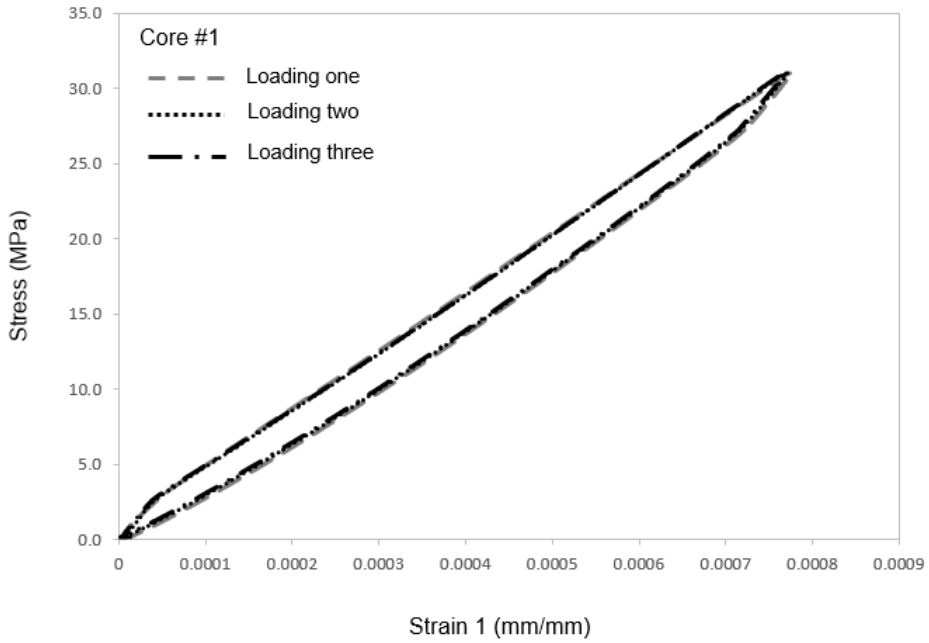

Figure 12. Typical stress-strain curve of concrete overlay core specimen under a constant loading rate (227 kg/sec).

A comparison of dynamic and static elastic modulus of core specimens is demonstrated in Fig. 13. The static elastic modulus tests were not conducted on Core #4 and Core #8 since they were tested to failure for compressive strength. In general, the dynamic modulus is significantly lower (average 25%) than the static modulus for core specimens acquired at experimental site. Several potential factors could contribute to the difference in modulus values:

- The static modulus is determined based on the measurements of core specimens of the concrete overlay. On the other hand, the dynamic modulus is determined based on the measurements of Rayleigh wave phase velocities with wavelength from 0.08 m to 0.3 m (including the concrete overlay, the intermediate asphalt layer as well as their interface).

Possible deterioration exists in the concrete overlay, intermediate asphalt layer or their interface could lead to the results of dynamic modulus reduction. A better correlation was identified when the PSPA test conducted on intact pavements, such as Core #3 and Core #6.

- The concrete could be anisotropic. Hence, the modulus determined by horizontally propagating stress waves could be less than that determined by compressive loading in the vertical direction. In addition, the mechanical properties of in-situ concrete and concrete cores could differ.

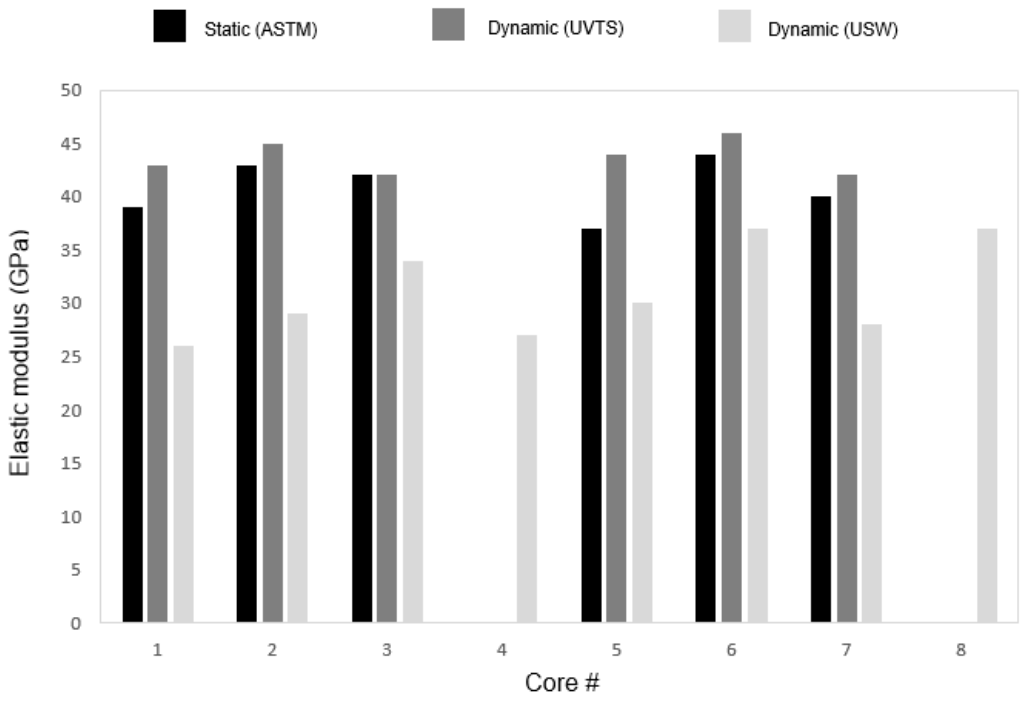

Figure 13. Comparison of elastic modulus of core specimens determined by different test methods.

Ultrasonic Velocity Testing Results

The compressional wave velocity (P-wave velocity) and dynamic elastic modulus of the concrete overlay for core specimens was measured in laboratory using an ultrasonic velocity test system. As shown in Fig. 14, the difference of first arrival time of P-waves can be calculated and used for estimating the P-wave velocity of concrete overlays based on Equation 4 with the measured length of the concrete overlay specimen. Then, the dynamic elastic modulus of concrete overlay can be estimated based on Equation 5 with the measured density of concrete overlay specimen.

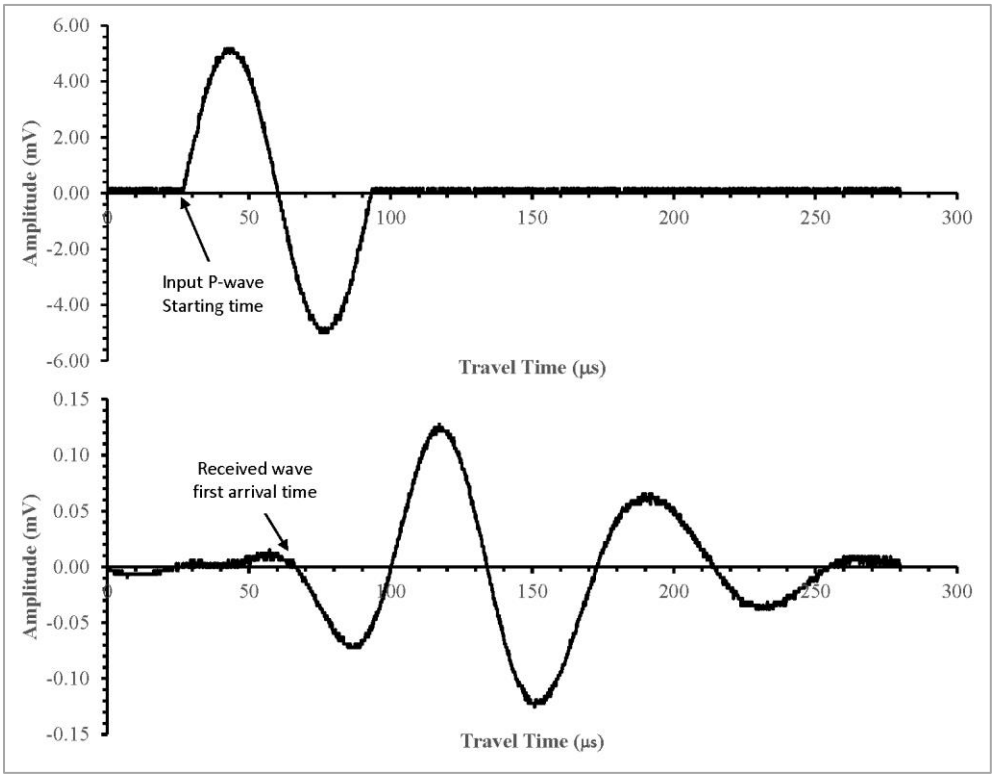

Figure 14. Typical input P-wave and received signals from ultrasonic velocity testing.

A comparison of the P-wave velocity of core specimens estimated based on ultrasonic velocity testing and PSPA-USW methods is shown in Fig. 15. An assumed value of Poisson's ratio of 0.18 for concrete was used to estimate the P-wave velocity of core specimens by the PSPA-USW method (Equation 3). The ultrasonic velocity tests were not conducted on Core #4 and Core #8 since they were tested to failure for compressive strength. In general, the P-wave velocity estimated by PSPA-USW tests is 14.5% (average) lower than the P-wave velocity estimated by the ultrasonic velocity tests.

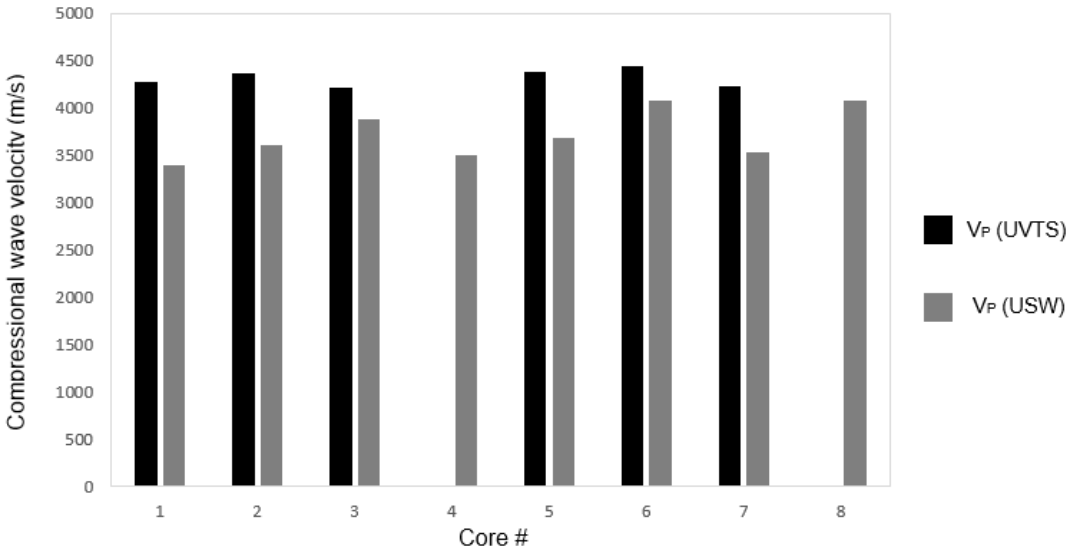

Figure 15. Comparison of compressional wave velocities of core specimens estimated by UVTS and PSPA-USW methods.

A comparison of the elastic modulus of core specimens estimated by three different test methods (ASTM C469, PSPA-USW and UVTS) is also shown in Fig. 13. A strong correlation between the static and dynamic elastic modulus of the concrete overlay

determined by laboratory testing methods was identified in Fig. 13. In general, the dynamic modulus is slightly higher (average 6.5%) than the static modulus for core specimens of the concrete overlay. On the other hand, the in-situ dynamic modulus of core specimens determined by the PSPA-USW method is significantly lower than the static modulus (average 25%) and laboratory dynamic modulus (average 30%). One possible reason that could lead to the modulus difference is that the in-situ dynamic modulus of core specimen was determined by measuring Rayleigh wave phase velocities with wavelengths from 0.08 m to 0.3 m, therefore, potential deterioration hidden in the concrete overlay, intermediate asphalt layer or their interface could affect the accuracy of the dynamic modulus. On the other hand, both laboratory tests were only conducted on core specimens of the concrete overlay, therefore, a potential defect in the intermediate asphalt layer or the concrete-asphalt interface will not affect the test result.

Due to the limitations of the number of core specimens, the quantitative correlations between the test results of each method cannot be established in this study. More core specimens are needed for further studies in order to verify the performance of the PSPA-USW method used for multi-layered pavement assessment, especially when the potential deterioration exists within each pavement layer or their interface.

PSPA-IE Test Results

Typical amplitude spectrum result of intact (Core #8) and debonded (Core #2) core specimens are shown in Fig. 16. In general, both amplitude spectra are dominated by flexural modes of vibration at low frequencies (2100 and 2800 Hz, respectively), which leads to a complicated spectrum where different frequency peaks are presented. In this

case, the thickness of the entire pavement cannot be estimated directly based on Equation 2. For intact core specimen (Core #8), the estimated thickness of the second (4400 Hz) and third (6000 Hz) frequency peaks were 460 mm and 340 mm on the basis of Equation 2 with an estimated P-wave velocity (Equation 3), which could be representative the reflectors from the bottom of the entire pavement (510 mm) and the interface of asphalt and basal concrete layers (280 mm). On the other hand, the second and third frequency peaks can still be identified in amplitude spectrum of debonded core specimen (Core #2) with relatively small amplitude values, is probably due to the influence of debonded interface.

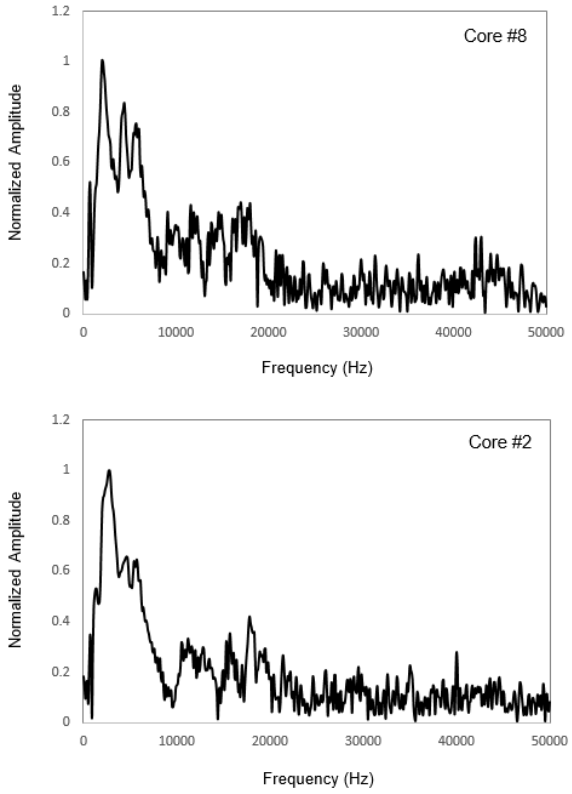

Figure 16. Typical amplitude spectrum result of intact (Core #8) and debonded (Core #2) core specimens.

Since the flexural mode of vibration was consistently identified in the amplitude spectra of all PSPA-IE test points acquired in this study, therefore, it is possible that the flexural mode vibration could be induced by multi-layering structure of the pavement, especially the asphalt and basal concrete layers which were designed to be unbonded.

In summary, the PSPA-IE method did not provide accurate estimates of either pavement layer thicknesses or depths to defects in this study. However, results suggest that defects can be inferred based on qualitative visual assessment of the amplitude spectrum. More creative thinking and future work is needed to improve the reliability of PSPA-IE thickness estimations in multi-layered pavement.

Conclusions

The PSPA device was used for first time for multi-layered pavement assessment in this case study. The performances and limitations of the PSPA were summarized based on the data presented and analyzed in this paper. More specifically:

- The PSPA-USW method can be used to assess the condition of concrete overlay, intermediate asphalt layer as well as their bonding conditions from a qualitative perspective. However, the Young's modulus of both concrete overlay and intermediate asphalt layer cannot be determined accurately on the basis of PSPA-USW test results, especially when a defect is present.
- A strong correlation between the static and dynamic elastic modulus of concrete overlay core specimens determined by laboratory testing methods was identified in this study. The dynamic modulus was slightly higher

(average 6.5 %) than the static modulus for core specimens of the concrete overlay. On the other hand, the in-situ dynamic modulus of core specimens determined by PSPA-USW method was lower than both the static modulus (average 25%) and laboratory dynamic modulus (average 30%).

- The PSPA-IE method did not provide accurate estimates of either the pavement layer thicknesses or the depths to defects due to the influence of flexural mode vibrations induced by multi-layering structure of pavement. Further work is needed in order to evaluate the performance of PSPA-IE method for multi-layered pavement assessment.

Acknowledgments

This work is performed under the support of the Missouri Department of Transportation (MoDOT) and the National University Transportation Center (NUTC) at the Missouri University of Science and Technology (Missouri S & T). The authors would like to acknowledge Kristian Krc, graduate student in civil department of Missouri S & T, for his assistance in the laboratory testing (ASTM - C469). The authors would also like to acknowledge Hongya Qu, graduate student in civil department at Missouri S & T, for his assistance in impact-echo data processing.

References

Baker, M., Crain, K., and Nazarian, S. 1995, Determination of pavement thickness with a new ultrasonic device: report for Texas Department of Transportation. Center for Highway Materials Research, University of Texas at El Paso, TX, 72 pp.

Baker, M., Nazarian, S., and Crain, K. 1997, Assessing quality of concrete with wave propagation techniques: ACI Materials Journal, 94, 296-306.

Cheng, C., and Sansalone, M. 1993, The impact-echo response of concrete plates containing delaminations: numerical, experimental and field Studies: Materials and Structures, 26, No. 5, 274-285.

Celaya, M., Shokouhi, P., and Nazarian, S. 2007, Assessment of debonding in concrete slabs using seismic methods: Transportation Research Record, 2016, 65-75.

Celaya, M., Nazarian, S., and Yuan, D. 2009, Comparison of field and laboratory strength of concrete slabs: in Expanded Abstracts: 7th International Symposium on Nondestructive Testing in Civil Engineering, Nantes, France, 1- 6.

Gibson, A., and Popovics, J. S. 2005, Lamb wave basis for impact-echo method analysis: Journal of Engineering Mechanics, 131, No. 4, 438 - 443.

Gucunski, N., Slabaugh, G., Wang, Z., Fang, T., and Maher, A. 2008, Impact echo data from bridge deck testing: Transportation Research Record, 2050, 111-121.

Hoda A., and Nazarian, S. 2015, Optimization of acoustic methods for condition assessment of concrete structures: ACI Materials Journal, 112, No. 4, 569-577.

Hertlein, B.H. 2013, Stress Wave Testing of concrete: A 25-year review a peek into the future: Construction and Building Materials, 38, 1240-1245.

Malhotra, V.M. and Carino, N. J. 2004, Handbook on Nondestructive Testing of Concrete 2th Ed: CRC Press LLC, West Conshohocken, PA, 177-179.

Popovics, J.S., Zemajtis, J., and Shkolnik, I. 2008, A Study of static and dynamic modulus of elasticity of concrete: ACI-CRC Final Report. University of Illinois, Urbana, IL, 16 pp.

Sansalone, M., and Streett, W.B. 1997, Impact-echo: nondestructive testing of concrete and masonry: Bullbrier Press, Jersey Shore, PA, 339 pp.

SECTION

2. CONCLUSION

From detailed experimental studies described and demonstrated in three papers, the following conclusions are drawn.

PSPA-USW is a rapid and fairly accurate method for estimating the in-situ elastic modulus (dynamic modulus) of concrete when the test wavelength range is shorter than the thickness of the concrete slab. However, defects identified in concrete, such as the delamination or the concrete degradation, could potentially affect the propagation of surface waves and the accuracy of dynamic modulus estimation. In addition, the bonding condition between the concrete and under layers, as well as the mechanical properties of the under layer material, could also affect the accuracy of dynamic modulus estimation if the full wavelength range is used for calculation the dynamic modulus of investigated pavement. In these situation, the obtained dynamic modulus of concrete is generally less accurate and refer to an apparent modulus.

PSPA-IE is a fairly accurate method for estimating the thickness of concrete slab. However, when the flexural mode vibration induced by shallow defects or other issues dominates the amplitude spectra, PSPA-IE method is not able to estimate depth of shallow defects. In addition, the estimation of P-wave velocity of concrete is less accurate when the full wavelength range is used for calculation the surface wave velocity of concrete. In this situation, the estimation of the thickness of concrete slab is generally less accurate. For multi-layered concrete pavement system (pavement thickness $\geq$ 20 in.), low frequency peaks consistent identified and dominated the amplitude spectra in most of

PSPA-IE test points. In this situation, PSPA-IE method is not able to estimate the thickness of entire pavements.

More creative thinking and future work is needed in order to improve the accuracy and reliability of both the USW and IE methods for characterizing and monitoring defects and mechanical properties of concrete infrastructures.

BIBLIOGRAPHY

Anderson, N.L., Sneed, L.H., Rosenblad, B., and Luna, R, "MoDOT Pavement Preservation Research Program Volume V. Site - Specific Pavement Condition Assessment," Report cmr16-004, Missouri Department of Transportation, 2015.

ASTM C 1383, "Test Method for Measuring the P-wave Speed and the Thickness of Concrete Plates using the Impact-Echo Method," 2000 Annual Book of ASTM Standards, Vol. 04.02, American Society of Testing Materials, West Conshohocken, PA.

Azari, H, "Optimization of Stress Wave-Based Nondestructive Methods in Identifying Deterioration in Concrete Structures," PhD Dissertation, University of Texas at El Paso, TX, 2013.

Azari, H., and Nazarian, S, "Optimization of Acoustic Methods for Condition Assessment of Concrete Structures," ACI Materials Journal, Vol. 112, pp 569-577, 2015.

Baker, M., Crain, R.K., and Nazarian, S, "Determination of Pavement Thickness with a New Ultrasonic Device," Research Report 1966-1. Center for Geotechnical and Highway Materials Research, University of Texas at El Paso, 1995.

Baker, M., Nazarian, S., and Crain, K, "Assessing Quality of Concrete with Wave Propagation Techniques," ACI Material Journal, Vol. 94, pp 296-305, 1997.

Carino, N.J., Sansalone, M., and Hsu, N.N, "A Point Source-Point Receiver Technique for Flaw Detection in Concrete," Journal of the American Concrete Institute, Vol. 83, No. 2, pp 199-208, 1986a.

Carino, N.J., and Sansalone, M, "Flaw Detection in Concrete using the Impact-Echo Method," Proceedings, NATO Conference on Bridge Evaluation, Repair and Rehabilitation, A.S. Nowak, Ed, Kluwer Academic Publishers, Dordrecht, Netherlands, pp 101-118, 1990.

Carino, N.J, "The Impact-Echo Method: An Overview," Proceedings of the Structures Congress & Exposition, American Society of Civil Engineers, Washington, D.C., 2001.

Cheng C.C., and Sansalone, M, "The Impact-Echo Response of Concrete Plates Containing Delaminations: Numerical, Experimental and Field Studies," Journal of Material Structure, Vol 26, pp 274-285, 1993.

Celaya, M., Shokouhi, P., and Nazarian, S. "Assessment of Debonding in Concrete Slabs using Seismic Methods," Transportation Research Record, Vol. 2016, pp 65-75, 2007.

Gucunski, N., Nazarian, S., Wiggenhauser, H., and Kutrubes, D, "Nondestructive Testing to Identify Concrete Bridge Deck Deterioration," Report S2-R06A-RR-1, Transportation Research Board, Washington D.C., 2013.

Li, M.X., Anderson, N., Sneed, L., and Maerz, N, "Application of Ultrasonic Surface Wave Techniques for Concrete Bridge Deck Condition Assessment," Journal of Applied geophysics, Vol. 126, pp 146-157, 2016.

Lin, J.M., and Sansalone, M.J, "Impact-Echo Studies of Interfacial Bond Quality in Concrete: Part I-Effects of Unbonded Fraction of Area," ACI Materials Journal, Vol. 93, No. 3, pp223-232, 1996.

Johanns, M., and Craig, J, "Pavement Maintenance Manual," Nebraska Department of Roads, 2002.

Krautkrämer, J., and Krautkrämer, H, Ultrasonic Testing of Materials, 4th Ed, Springer-Verlag, New York, 1990.

Malhotra, V.M., and Carino, N.J, Handbook on Nondestructive Testing of Concrete, 2th Ed, Chapter 14, CRC Press LLC, ASTM International, West Conshohocken, PA, pp 311-344, 2004.

Nazarian, S, "In situ Determination of Elastic Moduli of Soil Deposits and Pavement Systems by Spectral Analysis of Surface Waves Method," PhD Dissertation, The University of Texas at Austin, 1984.

Nazarian, S., and Stoke, K.H, "Use of Surface Waves in Pavement Evaluation," Transportation Research Record, National Research Council, Washington D.C., pp 132-144, 1986.

Nazarian, S., Yuan, D., Weissinger, E., and McDaniel, M, "Comprehensive Quality Control of Portland Cement Concrete with Seismic Methods," Transportation Research Record, Vol. 1575, pp 102-111, 1997.

Sansalone, M., and Carino, N.J, "Stress Wave Propagation Methods," in Handbook on Nondestructive Testing of Concrete, 1th Ed, CRC Press, Boca Raton, FL, pp 275-304, 1991.

Sansalone, M, "Impact-Echo: The Complete Story," ACI Structural Journal, Vol. 94, No. 6, pp 777-786, 1997.

Sansalone, M., and Streett, W.B, "Impact-Echo: Nondestructive Testing of Concrete and Masonry," Bullbrier Press, Jersey Shore, PA.

Sneed, L.H., Anderson, N.L., and Torgashov, E.V, "Nondestructive Evaluation of MoDOT Bridge Decks - Pilot Study," Report cmr14-010, Missouri Department of Transportation, 2014.

Zhu, J., and Popovics, J.S, "Imaging Concrete Structures using Air-Coupled Impact-Echo," Journal of Engineering Mechanics, Vol. 133, No. 6, pp 628-640, 2007.

Zhu, J., and Popovics, J.S, "Non-contact NDT of Concrete Structures using Air Coupled Sensors," Report No. NSEL-010, Newmark Structural Engineering Laboratory, University of Illinois at Urbana-Champaign, IL, 2008.

VITA

Mengxing Li was born in Yichang city, Hubei province, China. Between 2006 and 2010 he studied geology at the China University of Geosciences in Beijing. He received an M.S. in geological engineering from Missouri University of Science and Technology in May, 2012, and a Ph.D. in geological engineering from Missouri University of Science and Technology in May, 2017.